Atmos. Chem. Phys., 9, 7973–7995, 2009
www.atmos-chem-phys.net/9/7973/2009/

Atmospheric Chemistry and Physics

Properties of the average distribution of equatorial Kelvin waves investigated with the GROGRAT ray tracer

M. Ern[1], **H.-K. Cho**[2], **P. Preusse**[1], **and S. D. Eckermann**[3]

[1]Institute of Chemistry and Dynamics of the Geosphere (ICG-1), Forschungszentrum Jülich, Jülich, Germany
[2]Department of Atmospheric Sciences, Yonsei University, Seoul, Korea
[3]E.O. Hulburt Center, Naval Research Laboratory, Washington D.C., USA

Received: 16 March 2009 – Published in Atmos. Chem. Phys. Discuss.: 11 June 2009
Revised: 20 August 2009 – Accepted: 10 October 2009 – Published: 23 October 2009

Abstract. Kelvin waves excited by tropospheric convection are considered to be one of the main drivers of the stratospheric quasi-biennial oscillation (QBO). In this paper we combine several measured data sets with the Gravity wave Regional Or Global RAy Tracer (GROGRAT) in order to study the forcing and vertical propagation of Kelvin waves. Launch distributions for the ray tracer at tropospheric altitudes are deduced from space-time spectra of European Centre for Medium-Range Weather Forecasts (ECMWF) operational analyses, as well as outgoing longwave radiation (OLR) and rainfall data measured by the Tropical Rainfall Measuring Mission (TRMM) satellite. The resulting stratospheric Kelvin wave spectra are compared to ECMWF operational analyses and temperature measurements of the Sounding of the Atmosphere using Broadband Emission Radiometry (SABER) satellite instrument. Questions addressed are: the relative importance of source variability versus wind modulation, the relative importance of radiative and turbulent damping versus wave breaking, and the minimum altitude where freely propagating waves dominate the spectrum.

1 Introduction

Kelvin waves are the most prominent global scale equatorially trapped wave mode in atmospheric temperatures (e.g., Tindall et al., 2006a). They are symmetric with respect to the Equator, trapped at latitudes between about 20° S and 20° N in the stratosphere and travel eastward.

Like the other equatorially trapped planetary scale wave modes (e.g., equatorial Rossby or Rossby-gravity waves) Kelvin waves are forced in the tropical troposphere by deep convection (e.g., Salby and Garcia, 1987; Bergman and Salby, 1994; Pires et al., 1997; Straub and Kiladis, 2003; Lindzen, 2003; Randel and Wu, 2005). Therefore spectral signatures of Kelvin waves can be found in tropospheric space-time spectra of, for example, outgoing longwave radiation (OLR) or rain rates (e.g., Wheeler and Kiladis, 1999; Straub and Kiladis, 2003; Cho et al., 2004). These parameters are linked to the latent heat released in convective systems which is the source process of the wave generation (e.g., Salby and Garcia, 1987; Bergman and Salby, 1994; Ricciardulli and Garcia, 2000).

Kelvin waves can propagate vertically into the stratosphere. While the wave signal observed in the troposphere is located at relatively slow phase speeds and mostly directly coupled to the convective systems, Kelvin waves observed in the stratosphere are dominated by "free" wave modes, which are excited by deep convection in the troposphere but not longer linked with the space-time patterns of the convective forcing (Randel and Wu, 2005; Ern et al., 2008; Kiladis et al., 2009).

It has been demonstrated by Salby and Garcia (1987) how the atmospheric response in the near field (directly at the top of the heating source processes) is generated. It has also been shown by Garcia and Salby (1987) how the spectra of equatorial waves are changing in the far field: with increasing altitude the spectrum is shifted towards higher phase speeds due to wave damping processes.

Kelvin waves play an important role in the dynamics of the equatorial atmosphere. Together with other equatorial wave modes and a broad spectrum of gravity waves (GWs) Kelvin waves are one of the main drivers of the quasi-biennial oscillation (QBO) of the equatorial zonal wind in the stratosphere (Hitchman and Leovy, 1988; Dunkerton, 1997; Baldwin et al., 2001). Many processes in atmospheric chemistry and dynamics in the stratosphere and mesosphere (even at high latitudes) are modulated or influenced by the QBO, showing the importance of the driving equatorial wave modes like Kelvin waves (Baldwin et al., 2001).

Correspondence to: M. Ern
(m.ern@fz-juelich.de)

Published by Copernicus Publications on behalf of the European Geosciences Union.

Further processes Kelvin waves are important for are the mean upwelling observed in the equatorial region (e.g., Semeniuk and Shepherd, 2001) as well as mixing processes both vertically (e.g., Fujiwara et al., 1998; Fujiwara and Takahashi, 2001) and across the subtropical mixing barrier, which is more stable during QBO easterly phases (e.g., Shuckburgh et al., 2001). In addition, they play an important role for the dehydration of the tropical tropopause region (e.g., Fujiwara et al., 2001; Zhou and Holton, 2002; Hatsushika and Yamazaki, 2003; Eguchi and Shiotani, 2004; Jensen and Pfister, 2004; Immler et al., 2008).

Because Kelvin waves interact with the QBO winds Kelvin wave activity itself is modulated by the QBO. Enhanced Kelvin wave activity is observed during QBO westward phases when the propagation conditions are favorable for eastward traveling waves. According to conventional wisdom Kelvin waves are subjected to enhanced radiative damping when they approach the zonal wind reversal from westward to eastward wind, and accordingly transfer momentum to the background wind thus contributing to the reversal of the zonal wind direction (e.g. Holton and Lindzen, 1972; Campbell and Shepherd, 2005a,b).

In contrast, GWs are assumed to transfer momentum by either absorption at critical levels (e.g., Lindzen and Holton, 1968; Campbell and Shepherd, 2005a,b) or breaking on reaching their saturation amplitudes (e.g., Campbell and Shepherd, 2005a,b). Therefore GW parameterizations (e.g., Hines, 1997a; Alexander and Dunkerton, 1999; Warner and McIntyre, 2001) do not take into account radiative damping. However, in the tropics Kelvin waves and gravity waves share the same dispersion relation

$$\hat{\omega} = -N\,k/m, \tag{1}$$

with $\hat{\omega}$ the intrinsic frequency of the wave, N the buoyancy frequency, k the horizontal, and m the vertical wavenumber of the wave. I.e., Kelvin waves are in principal GWs confined to the tropics by the Coriolis force. The only difference is their horizontal wavelength and hence their group velocity

$$c_{gz} = \frac{\partial\hat{\omega}}{\partial m} = \frac{Nk}{m^2} = \frac{k\,\hat{c}_h^2}{N}, \tag{2}$$

which is for waves of the same horizontal phase speed $\hat{c}_h{=}\hat{\omega}/k$ proportional to the horizontal wavenumber k. This means that for long horizontal wavelength GWs radiative forcing must be important and, on the other hand, that wave saturation could become important for higher wavenumber Kelvin waves.

Studies on the QBO and its driving by different equatorial wave modes were either highly idealized (e.g. Lindzen and Holton, 1968; Holton and Lindzen, 1972; Dunkerton, 1997; Campbell and Shepherd, 2005a,b) or were based on complex general circulation model (GCM) simulations (Horinouchi et al., 2003; Giorgetta et al., 2006; Mayr et al., 2007) providing little insight in the detailed mechanisms and based on only partially realistic convective forcing (Ricciardulli and Garcia, 2000; Horinouchi et al., 2003). Highly idealized simulations which assume for instance only a single wavenumber 1 Kelvin wave and a continuous omnipresent forcing were justified in terms of thought experiments. In addition, only little was known about the spectrum of Kelvin waves and its temporal variations. However, improved satellite sensors recently provide these information for the troposphere (e.g., Wheeler and Kiladis, 1999; Straub and Kiladis, 2003; Cho et al., 2004) as well as for the stratosphere (Ern et al., 2008; Alexander et al., 2008) and the mesosphere (Garcia et al., 2005; Ern et al., 2009). In our work we additionally use European Centre for Medium-Range Weather Forecasts (ECMWF) analyses which assimilate tropospheric measurements of convection and rain rates and have been validated to well represent also the stratospheric Kelvin wave amplitudes (Ern et al., 2008) and also Kelvin wave fluxes and zonal wind forcing have been found to be in good agreement with measurements (Ern and Preusse, 2009).

For driving the QBO or the tropical upwelling we need to know the wave forcing, i.e. the vertical derivative of the momentum flux. This means that even data sets displaying on average roughly the same Kelvin wave amplitudes can produce different forcing if the vertical gradients differ. In addition, the interaction between waves and background winds is non-linear in nature. Therefore both the intermittency of the wave sources and the details of the interaction with the background wind are important.

In order to interpret all measurements available for the troposphere and the stratosphere in a synergetic approach we use the Gravity wave Regional Or Global RAy Tracer (GROGRAT) model. GROGRAT calculates the upward propagation of waves according to the ray tracing equations and conserves wave action density along the ray path. In addition, the model includes dissipation of wave amplitudes through wave breaking (wave saturation) due to convective and dynamical instabilities (Fritts and Rastogi, 1985), vertical scale-dependent infrared radiative damping (Zhu, 1993), and climatological background vertical diffusivities (for details see Marks and Eckermann, 1995, and Eckermann and Marks, 1997). In the GROGRAT model we have complete control over these dissipative processes and can perform model experiments investigating the influence of the various damping mechanisms. In addition, we can freely vary the launch distribution and launch altitude of the waves.

We first describe the space-time analysis and the set-up of the GROGRAT model in Sect. 2. In Sect. 3 we will investigate the importance of radiative and turbulent damping for the interaction of the Kelvin waves with the zonal background winds. In Sects. 4 and 5 we will study the impact of different source spectra and launch altitudes on the distribution of Kelvin waves observed in the stratosphere. In addition, the influence of seasonal variations in the tropospheric Kelvin wave source on the stratospheric variability is demonstrated. The results are summarized in Sect. 6

2 Method: Kelvin wave spectra and simulation with GROGRAT

2.1 Theory of equatorial Kelvin waves

A theoretical description of planetary scale equatorial wave modes was first given by Matsuno (1966) who derived the properties of the different equatorially trapped wave types from solutions of the shallow-water model on an equatorial beta plane.

One important parameter is the so called equivalent depth h_e. The equivalent depth is connected with the vertical wavenumber m as given in Eq. (3) (e.g., Wu et al., 2000; Lindzen, 2003):

$$m^2 = \left(\frac{N^2}{g\, h_e} - \frac{1}{4H^2} \right) \tag{3}$$

with N the buoyancy frequency, g the gravity acceleration, and H the pressure scale height.

One of the most prominent global scale equatorial wave modes are Kelvin waves. The dispersion relation for Kelvin waves is given by:

$$\hat{\omega} = -\sqrt{g\, h_e}\, k \approx -N\, k/m \tag{4}$$

with $\hat{\omega}$ the intrinsic frequency of the wave, and k the zonal wavenumber. From Eq. (4) we see that the phase speed $\hat{\omega}/k$ of a Kelvin wave is directly coupled with the equivalent depth. Under the assumption of zero background wind equivalent depths of 8, 90 and 2000 m correspond to intrinsic phase speeds of 9, 30, and 140 m/s (see Eq. 4) and vertical wavelengths of about 3, 9 and 50 km in the stratosphere, or about 6, 19 and 100 km in the troposphere due to the lower buoyancy frequency N there (see Eq. 3).

It should be noted that the frequencies ω that are observed by satellite instruments and most other observing systems are ground based (Eulerian) frequencies. These frequencies remain unchanged in cases of non-zero background wind and spectral features in ground based frequency/zonal wavenumber spectra like in our paper are not Doppler shifted. On the other hand intrinsic wave frequencies $\hat{\omega}$ will be Doppler shifted in case of non-zero background wind according to:

$$\hat{\omega} = \omega - k\, \bar{u} \tag{5}$$

with k the horizontal wavenumber and $\bar{u}$ the background wind. Also the vertical wavelength of the waves considered will be Doppler shifted. A more detailed discussion can, for example, be found in Ern et al. (2008).

2.2 Space-time spectra of Kelvin waves

Equatorially trapped global scale wave modes are either symmetric or antisymmetric with respect to the Equator. Therefore often measured or modeled data fields are divided into symmetric and antisymmetric components. Every data field $\Psi(\lambda, \Phi, t)$ can be written as sum of its symmetric $\Psi_{\text{symm}}(\lambda, \Phi, t)$ and its anti-symmetric $\Psi_{\text{anti}}(\lambda, \Phi, t)$ parts (λ: longitude, Φ: latitude, t: time):

$$\begin{aligned} \Psi(\lambda, \Phi, t) = & \tfrac{1}{2}(\Psi(\lambda, \Phi, t) + \Psi(\lambda, -\Phi, t)) \\ & + \tfrac{1}{2}(\Psi(\lambda, \Phi, t) - \Psi(\lambda, -\Phi, t)) \\ =: & \Psi_{\text{symm}}(\lambda, \Phi, t) + \Psi_{\text{anti}}(\lambda, \Phi, t) \end{aligned} \tag{6}$$

In a similar way also symmetric and antisymmetric space-time Fourier spectra $\hat{\Psi}_{\text{symm}}(k, \omega; \Phi)$ and $\hat{\Psi}_{\text{anti}}(k, \omega; \Phi)$ can be calculated for every latitude Φ. Both symmetric and antisymmetric components have to be treated independently. This method has been used in several studies based on tropospheric (e.g., Wheeler and Kiladis, 1999; Cho et al., 2004) as well as stratospheric data (e.g., Ern et al., 2008; Alexander et al., 2008).

This technique has the advantage that the different wave modes can be separated more easily. In addition, in symmetric and antisymmetric spectra the background noise due to non-resolved waves is lower than it would be in a "full" Fourier spectrum containing all spectral contributions. This is the case because the background variances are split up into a symmetric and an antisymmetric background, each lower than the background of the "full" spectrum. Usually both symmetric and antisymmetric spectra are averaged over a latitude interval centered at the Equator to further increase the signal to noise ratio of the single spectral components.

In our study we follow the method described in Ern et al. (2008). But since our paper is focused on Kelvin waves alone, we will only treat symmetric spectra and positive frequencies (i.e., eastward propagating waves).

Like in Ern et al. (2008) and Ern and Preusse (2009) we use residual ECMWF analysis temperatures gridded down to 9° resolution in longitude from originally 1°, resulting in a maximum zonal wavenumber of 20 that can be resolved. The original resolution of 1° meridionally has been retained unchanged and space-time spectra are calculated for each latitude in 1° steps. Frequencies up to 2 cycles/day can be resolved since the ECMWF analyses are available every 6 h at 00:00, 06:00, 12:00, and 18:00 GMT. The symmetric spectra used in our work are meridional averages over the spectra calculated at the latitudes from 15° S to 15° N. The ECMWF data set is given on a set of pressure levels which we convert to pressure altitudes using a constant scale height of 7 km.

In Sects. 3, 4, and 5 we also use Kelvin wave variances derived from Sounding of the Atmosphere using Broadband Emission Radiometry (SABER) temperature space-time spectra as a reference. The SABER instrument onboard the Thermosphere Ionosphere Mesosphere Energetics and Dynamics (TIMED) satellite measures temperatures and several trace gases from the tropopause region to above 100 km (e.g., Mlynczak, 1997; Russell et al., 1999; Yee et al., 2003). Like in Ern et al. (2008) we use version 1.06 temperature data, and the space-time spectra are calculated from residual temperatures and averaged over the latitudes from 12° S to

12° N in 4° steps, according to the horizontal sampling distance of about 500 km along the satellite track. Due to the orbit geometry of the TIMED satellite zonal wavenumbers up to 6–7 and frequencies up to 1 cycle/day can be resolved by the asynoptic sampling. The SABER data used are given on fixed geometric altitudes from 15 km to above 100 km in 1-km steps. This is somewhat better than the vertical resolution given by the instantaneous vertical field-of-view of about 2 km.

Different from Ern et al. (2008) our analysis will be based on non-overlapping time windows of 36 days for the Fourier analysis of ECMWF and SABER temperatures because in Sect. 5 we want to directly compare to results based on space-time spectra calculated from OLR and rainfall rates measured by the Tropical Rainfall Measuring Mission (TRMM) satellite which were calculated using 96-day time windows stepped forward in 36-day steps (Cho et al., 2004). The center times of the 36-day windows were chosen to exactly match the center times of the 96-day windows.

2.3 Simulation of Kelvin wave spectra with GROGRAT

For the initialization of a GROGRAT ray tracer model run several input parameters have to be provided. First, the wind amplitude and propagation direction, as well as the ground based phase speed of the wave ω/k have to be specified. Second, an atmospheric background profile has to be defined.

Because Kelvin waves have no meridional wind component we need only zonal wind amplitudes and the propagation direction will always be eastward.

Even though one of the required input parameters is a wind amplitude, in our study we will mainly rely on ECMWF temperature spectra. One reason is that the ECMWF temperature spectra were directly validated with measured SABER temperature spectra by Ern et al. (2008) and Ern and Preusse (2009), whereas the quality of ECMWF wind spectra has not been validated by measurements so far. There are some indications that ECMWF zonal wind spectra are less reliable and less suited for the analysis of Kelvin waves (see Sect. 4). In particular, in temperature spectra the Kelvin wave signal will be the by far most prominent spectral component and less contaminated by other waves than in wind spectra (see also Tindall et al., 2006a,b). Another reason is that we also want to use SABER temperature spectra or derived Kelvin wave variances for comparison with the results of our simulations in Sects. 3, 4, and 5.

Therefore we choose to calculate pseudo zonal wind spectra from the temperature spectra which can easily be done via the polarization relations for Kelvin waves using the following equation:

$$|\tilde{u}| = \left|\frac{k}{\hat{\omega}}\right| \frac{|T'|}{T} \Big/ \sqrt{\left[\frac{\gamma}{c_s^2} - \frac{1}{2gH}\right]^2 + \left[\frac{Nk}{g\,\hat{\omega}}\right]^2} \qquad (7)$$

Here $\tilde{u}$ is the zonal wind amplitude of the Kelvin wave, T' the temperature amplitude, and T the background temperature, c_s the speed of sound, and γ=1.4 the adiabatic coefficient. For a derivation of Eq. (7) see Appendix A.

This transformation of temperature amplitudes into pseudo zonal wind amplitudes can be done for both ECMWF and SABER temperature spectra, and in the following all ECMWF and SABER spectra shown are spectra of pseudo zonal wind amplitudes and wave variances shown are pseudo wind variances calculated from these spectra.

These pseudo zonal wind spectra can directly serve as input for the GROGRAT ray tracer. For each of the independent spectral grid points we can calculate the required ground based phase speed from the given zonal wavenumber and frequency. The spectral amplitudes of the Fourier spectra can be directly taken as launch amplitudes for the ray tracer.

In our study we only use latitudinally averaged spectra and are only interested in the global average evolution of Kelvin waves. For this reason, and also to be consistent with our source spectra, GROGRAT is run in an ECMWF background atmosphere (temperature and winds) averaged over the 36-day time-windows of the Fourier analysis and over the latitude range 15° S–15° N. In addition, since we consider only latitudinally averaged global scale waves, in GROGRAT we allow only vertical propagation of the waves.

This means that different from the general ray tracing approach no horizontal propagation or refraction are included in our simulations. For the vertical propagation, however, we still rely on the ray tracing approach, and the vertical evolution of the vertical group velocity and the propagation time are crucial for the amount of radiative and turbulent damping taking effect, and hence, whether wave saturation is reached. And we also make use of the well established algorithms developed for the GROGRAT ray tracer.

The use of these algorithms is of great practical value since by using the GROGRAT ray tracer we have full control on the wave dissipation processes. In our simulation wave saturation due to both static and dynamic instabilities are included via a scheme based on the work by Fritts and Rastogi (1985). For low frequency waves like in our case the saturation amplitudes are the same as for the more generalized approach described by Marks and Eckermann (1995) which is based on the work by Hines (1988). In addition, vertical scale-dependent infrared radiative damping (Zhu, 1993), and climatological background vertical diffusivities are included in the GROGRAT model (for details see Marks and Eckermann, 1995, and Eckermann and Marks, 1997).

It should be noted that the wave amplitude calculation for gravity waves used in GROGRAT may be used as a first order approximation to simulate the vertical propagation of planetary-scale Kelvin waves. However large scale effects like 2d flow effects, critical layers in latitudinal shear etc. are not covered and require different concepts. In addition, the concept of localized wave packets used for gravity waves makes no sense for planetary scale waves.

It should also be stated clearly that we make several simplifications that allow only in a first order approach to study

the basic mechanisms of the average global Kevin wave distribution and its interaction with the QBO. For example, we assume a zonal background wind that is uniform, in both zonal and meridional coordinates within the analyzed latitudinal range, and also the global distribution of Kelvin waves is assumed to be uniform in our simulations (both at the source level and also above). However, it is known that the global distribution of Kelvin waves is not uniform in the troposphere (for example, due to the Walker circulation) and this will affect the distribution of stratospheric Kelvin waves propagating both eastward and upward from the troposphere (e.g., Suzuki and Shiotani, 2008; Kawatani et al., 2009). Non-uniform distributions of Kelvin waves in the stratosphere have been found, for example, by Alexander et al. (2008) or Ern et al. (2008). Another effect that is neglected is that Kelvin waves can have a meridional wind component in a sheared background wind (see Imamura, 2006, and references therein).

Nevertheless, although neglecting those effects will introduce some bias in the results of our simulations this will likely not affect the key findings of our study, which are rather of qualitative than of quantitative nature.

3 The role of wave saturation, radiative and turbulent damping for the vertical evolution of Kelvin wave spectra

The importance of radiative damping for the dissipation of Kelvin waves has been pointed out by Holton and Lindzen (1972) already some years after the discovery of Kelvin waves in the atmosphere by Wallace and Kousky (1968).

The GROGRAT ray tracer calculates both saturated and unsaturated wave amplitudes. A comparison of saturated and unsaturated amplitudes allows to study the role of wave breaking. In addition, the physical processes of radiative and turbulent wave damping can be switched on or off. These options will be used to investigate the role of wave damping and breaking for the observed shift of the Kelvin wave spectral signatures towards higher phase speeds with altitude.

3.1 Vertical evolution of ECMWF spectra

In our studies ECMWF space-time spectra are used both as spectral source distributions and as references for GROGRAT simulations. Figure 1 shows symmetric ECMWF pseudo zonal wind spectra averaged over the whole 5-year period (January 2002–November 2006) considered in our study at different altitudes from about 4.9 to 18.7 km in the troposphere and lower stratosphere. Please note that in Fig. 1 not the full spectral range covered by the ECMWF data set is shown (see Sect. 2.2). These spectra will also be used as source distribution in Sect. 4.3 and the spectrum shown in Fig. 1e will be used below.

Very high amplitudes can be found at low frequencies and only at higher altitudes the lobe-shaped spectral feature due to Kelvin waves known from observations in the stratosphere (e.g., Ern et al., 2008) starts to develop. For comparison also the lines for equivalent depths 8, 90, and 2000 m (values given assume zero background wind) are shown as straight lines through the origin. These lines correspond to ground based phase speeds ω/k of about 9, 30, and 140 m/s.

Spectral signatures of Kelvin waves in the troposphere are usually found in a spectral band between the lines of 8 and 90 m equivalent depth (Wheeler and Kiladis, 1999). The higher up in the stratosphere the more this spectral feature is shifted towards higher phase speeds. This shift can be seen in Fig. 2a–c showing symmetric pseudo zonal wind spectra calculated from ECMWF temperature spectral amplitudes in the stratosphere at the altitudes 21.1 km (a), 30.0 km (b), and 40.8 km (c).

The stratospheric ECMWF spectra shown in Fig. 2a–c were validated by comparison with SABER measurements (see Ern et al., 2008) and can therefore be taken as reference for our GROGRAT simulations

3.2 Vertical evolution of simulated GROGRAT spectra with standard settings

The same spectra as in Fig. 2a–c were simulated with the GROGRAT ray tracer using the method described in Sect. 2.3. The 5-year average spectrum shown in Fig. 1e is taken as constant source distribution at 16.9 km altitude (about the tropopause height in the tropics). In this and in all other simulations we use an ECMWF background atmosphere which is different for each of the 36-day time windows of our analysis, but averaged in longitude, the latitude range used, and the whole time window (see Sect. 2.3).

The spectra resulting from a GROGRAT simulation based on the GROGRAT standard settings were averaged over the period January 2002–November 2006 and are shown in Fig. 2d–f. It can be seen that indeed the lobe-shaped spectral feature develops in the stratosphere even though only weakly indicated in the source distribution (Fig. 1e). Part of the wave components at low phase speed are damped and dissipate near critical levels while the amplitudes of higher phase speed waves grow with altitude due to decreasing atmospheric density and become visible. This explains the lobe-shaped structure of the Kelvin wave spectral peak as well as the shift towards higher phase speeds with altitude.

Shape and amplitudes of this spectral feature are about the same as in the ECMWF spectra given as a reference in Fig. 2a–c. Only at the highest altitude of 40.8 km the GROGRAT simulation shows some high bias at high frequencies, maybe indicating that the linear dissipation processes parameterized in GROGRAT are not strong enough. Indications that also nonlinear processes can be involved in the dissipation of gravity waves, in particular in the process of wave breaking, has been shown, for example, by Achatz (2007).

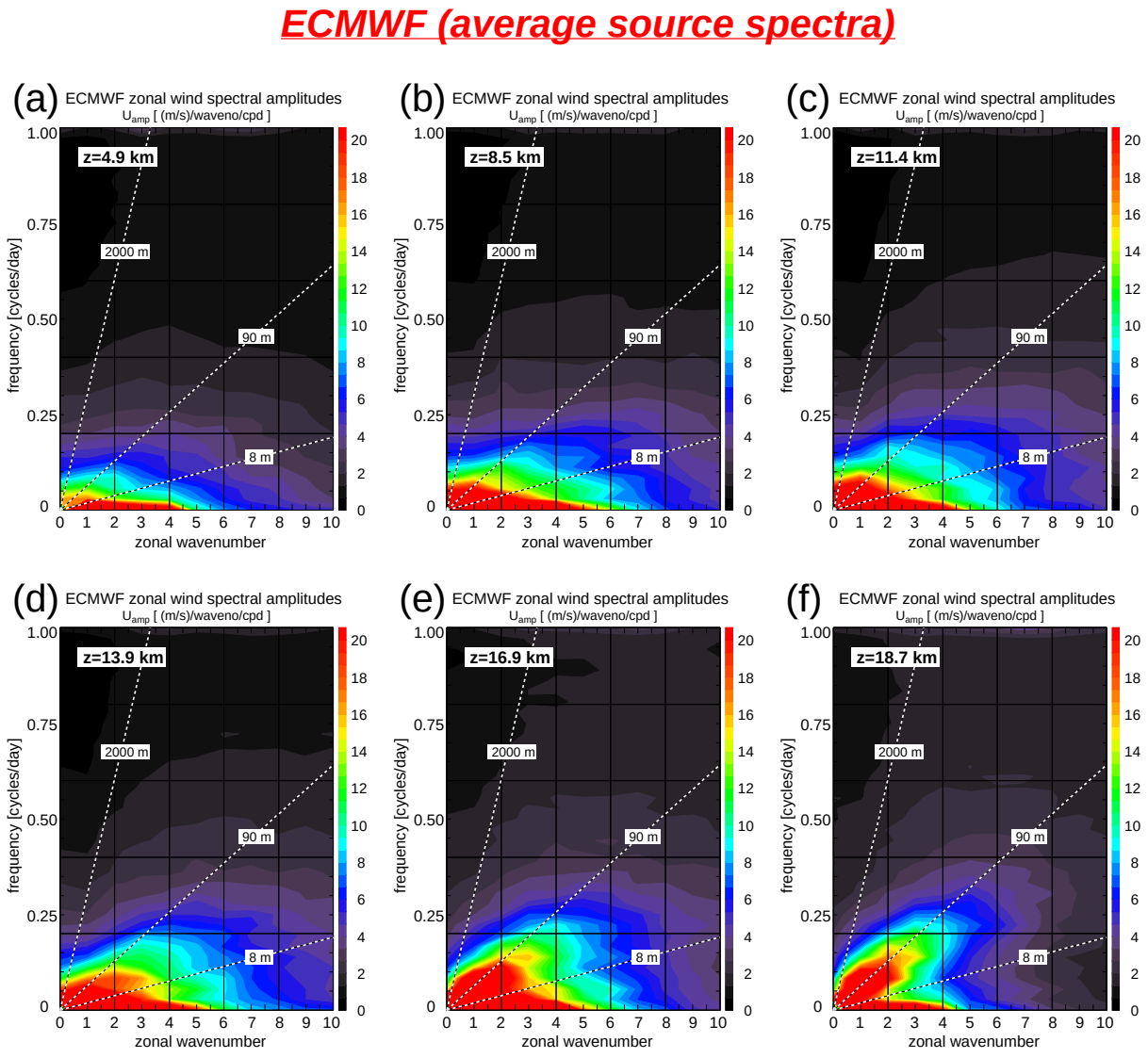

Fig. 1. ECMWF pseudo zonal wind spectra averaged over the period January 2002–November 2006 for the altitudes 4.9 km **(a)**, 8.5 km **(b)**, 11.4 km **(c)**, 13.9 km **(d)**, 16.9 km **(e)**, and 18.7 km **(f)**. Also given are the lines for equivalent depths h_e=8, 90, and 2000 m, corresponding to ground based phase speeds of 9, 30, and 140 m/s.

The role of wave saturation for Kelvin waves will therefore be discussed in the next subsection.

3.3 The role of wave breaking

Amplitude limits critical for wave breaking are never reached in our simulations. This can be seen by comparing saturated and unsaturated GROGRAT amplitudes, which are always exactly the same. This means that wave dissipation takes place only by radiative and turbulent damping as well as critical level filtering.

GROGRAT does not support the superposition of different waves and as a consequence different spectral components are treated independently in our simulations. However, the amplitude limit critical for the onset of wave breaking could also be reached by a superposition of different waves. Therefore we make another cross-check whether the critical amplitude limit is really never reached.

Investigation of ECMWF analysis pseudo zonal wind spectra shows that in the altitude range of about 20–50 km about 4 spectral components are required to describe 50% of the total variance due to Kelvin waves for equivalent depths between 8 and 2000 m. These results were obtained from the single (not time-averaged) spectra calculated in the 36-day time windows mentioned above. About 10 spectral components are required to describe about 80% of the Kelvin wave variances.

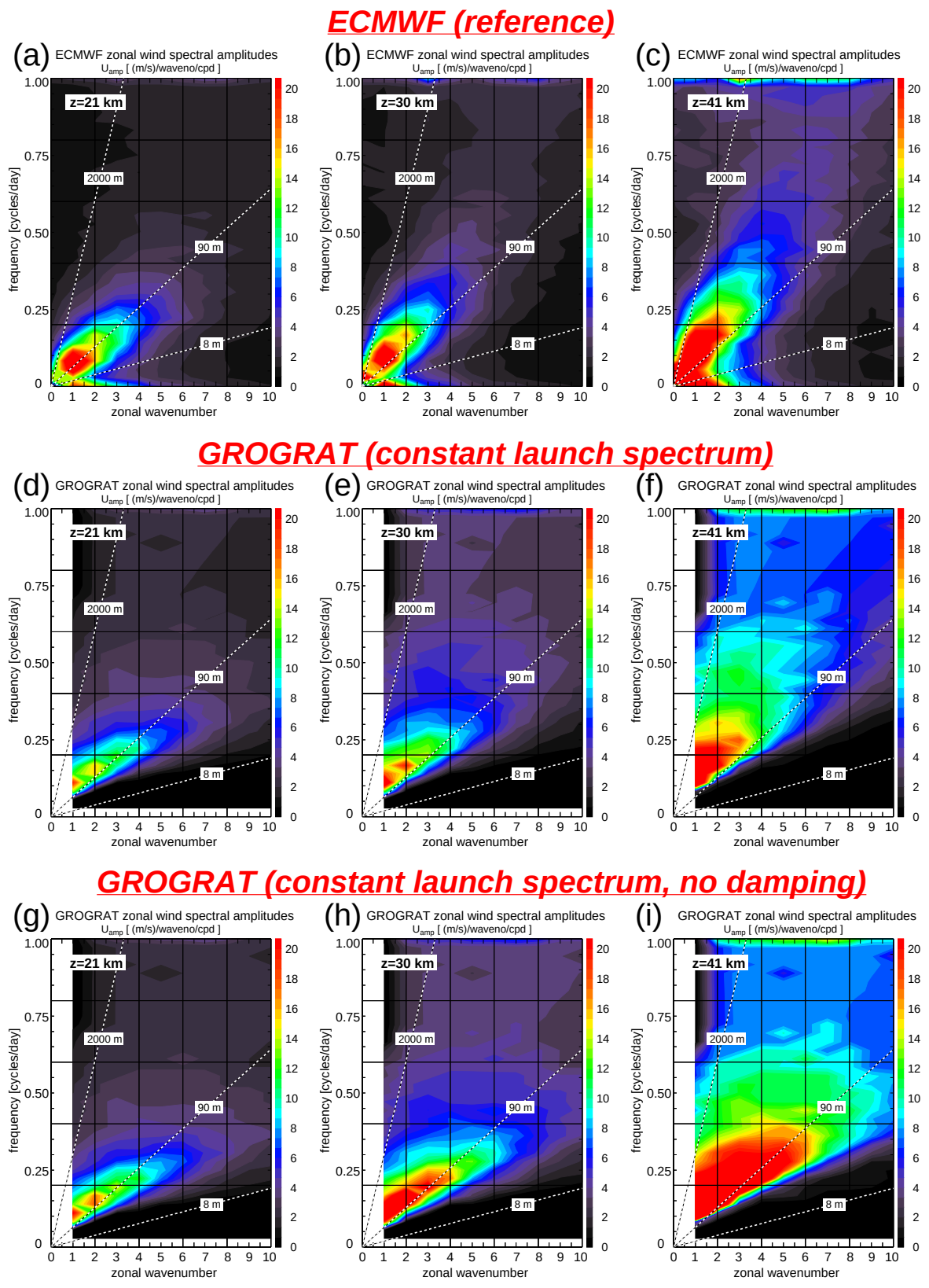

Fig. 2. ECMWF pseudo zonal wind spectra averaged over the period January 2002–November 2006 for the altitudes 21.1 km **(a)**, 30.0 km **(b)**, and 40.8 km **(c)**. Also shown the same spectra simulated with GROGRAT using standard settings **(d)**–**(f)** and with radiative and turbulent damping switched off in GROGRAT **(g)**–**(i)**.

Therefore we checked whether critical amplitude limits are still not reached if the source amplitudes of the GROGRAT simulations are multiplied by a factor of 10. In this way also the possibility of constructive wave superposition of the different relevant spectral components is taken into account. This is a very conservative assumption because different spectral components more likely will have different phases and different ground based phase speeds so that there will be an averaging effect at a given altitude. In spite of this conservative assumption the critical amplitude limit is still not reached in the relevant altitude range from about 20–50 km. The amplitudes are well below the amplitude limit critical for wave breaking, indicating that the assumptions made in our simulations do not influence the results shown and that radiative and turbulent damping are the most important wave dissipation processes for Kelvin waves in the considered altitude range.

3.4 Some cross-checks relevant for the spectral shape

3.4.1 Vertical evolution of simulated GROGRAT spectra with damping switched-off

Figure 2g–i shows the same spectra as in Fig. 2d–f but resulting from a GROGRAT simulation with radiative and turbulent damping switched off. We still find some kind of lobe-shaped spectral peak because the waves with the lowest phase speeds also stall vertically near critical levels. But with increasing altitude the amplitude of the spectral peak becomes unrealistically high, and at 40.8 km altitude the peak is too broad, covering a too large zonal wavenumber range and extending towards too high frequencies. Although the amplitudes are no longer damped critical amplitude limits are not reached and wave breaking does not take effect.

3.4.2 Time-varying source spectra

Both GROGRAT simulations (with wave damping switched on as well as off) were also carried out with time-varying ECMWF source spectra: for each of the 36-day time-windows the corresponding ECMWF spectrum at 16.9 km altitude was taken as source spectrum, instead of the 5-year average ECMWF spectrum. However, also for this simulation based on those time-varying ECMWF source spectra the simulated 5-year average spectra at 21.1, 30.0, and 40.8 km altitude almost look the same as in Fig. 2d–i and are not shown.

3.4.3 Compatibility of vertical wavelength ranges

Another cross-check was made, whether visibility filtering of the GROGRAT simulations is required to remove Kelvin waves with vertical wavelengths too short to be contained in the ECMWF analyses, or too short to be visible by the SABER satellite instrument, since these two data sets will be used as a reference in Sects. 4 and 5. However, already shortly after launch vertical wavelengths shorter than about 5 km are removed from the space-time spectra and the results filtered for vertical wavelengths longer than 5 km and results without vertical wavelength filtering are almost the same. This means that all Kelvin waves contained in our GROGRAT simulations should also be contained in ECMWF or be visible for SABER, and the calculated Kelvin wave variances can be directly compared because about the same vertical wavelength ranges are covered by the different data sets.

3.5 Radiative versus turbulent damping

We also investigated the relative importance of radiative and turbulent damping. Kelvin wave pseudo zonal wind variances were calculated by integrating over the power spectra for wavenumbers 1–6 between the lines of equivalent depths of 8 and 2000 m for Kelvin waves and frequencies lower than 0.4 cycles/day (see also Sect. 4). The so obtained variance altitude profiles for each 36-day window were then averaged over the whole period January 2002–November 2006.

The resulting average profiles are shown in Fig. 3. As a reference the variances obtained directly from space-time spectra of ECMWF operational analyses (black solid line) and SABER measurements (black dashed line) are given. Also given are integrated and then averaged variances resulting from GROGRAT simulations based on time-varying ECMWF source spectra at 16.9 km source altitude with full damping switched on (green dotted), radiative damping only (blue dotted), and no damping at all (red dotted).

Obviously the simulation including both radiative and turbulent damping (green dotted) closely follows the ECMWF and SABER reference curves. There is some low bias around the source altitude because GROGRAT does not propagate upward very low phase speed spectral components of the ECMWF source spectra, which are removed in the simulated GROGRAT spectra directly after launch. These red parts of the source spectra are caused partly by very short vertical wavelength Kelvin waves which are not important at higher altitudes, and partly by red noise due to unorganized convection. In addition, there is also some high bias above 45 km altitude, which is however removed if the source altitude is chosen higher than 20 km (not shown).

One possible reason for the reduction of this high bias at high altitudes could be that the higher the source altitude is chosen the more "noise" in the source spectra caused by non-Kelvin wave contributions is removed. If such "noise" is located at higher phase speeds it can grow considerably with altitude without being dissipated in our simulation. For source altitudes above 20 km this "noise" is likely small and the bias at high altitudes will be reduced.

Variances resulting from the GROGRAT simulation with radiative damping only (blue dotted) are only slightly higher than for the full damping case (green dotted). If also radiative damping is switched off (red dotted) variances are

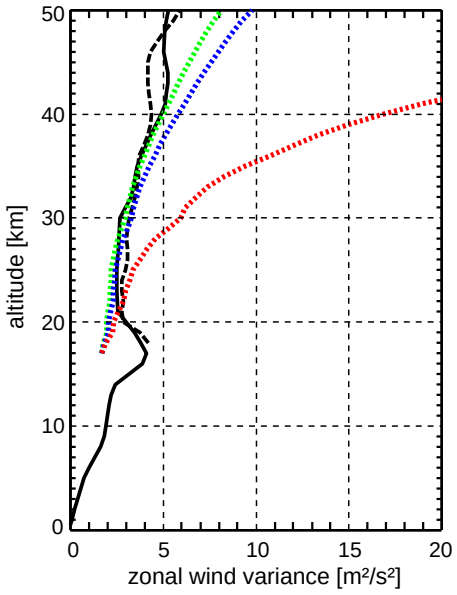

Fig. 3. Altitude profiles of Kelvin wave pseudo zonal wind variances obtained by integrating over the power spectra for wavenumbers 1–6 (the range of wavenumbers available for SABER) between the lines of equivalent depths of 8 and 2000 m for Kelvin waves and frequencies lower than 0.4 cycles/day and then averaged over the whole period January 2002–November 2006. Shown are variances from ECMWF operational analyses (black solid line) and from SABER measurements (black dashed line) as references (see also Fig. 4). Also shown are integrated and then averaged variances obtained from GROGRAT simulations with time-varying ECMWF source spectra at 16.9 km source altitude with the following setups: (1) full damping (radiative and turbulent) switched on (green dotted), (2) radiative damping only (blue dotted), and (3) no damping at all (red dotted). For details see text.

considerably higher than in the full damping case. This indicates that for Kelvin waves the main damping process is radiative damping, and turbulent damping plays only a minor role.

4 GROGRAT simulation of Kelvin wave variances based on ECMWF source spectra

4.1 Consistency check with stratospheric ECMWF source distribution

One method to derive temperature variances due to Kelvin waves is to integrate over the spectral band characteristic for this kind of waves (see Ern et al., 2008). In a similar way variances are derived from pseudo zonal wind spectra calculated via the polarization relations for Kelvin waves from ECMWF and SABER temperature spectra. The spectral band we use has already been introduced in Sect. 3.5: the zonal wind variances were obtained by integrating over the power spectra for wavenumbers 1–6 (the range of wavenumbers available for SABER) between the lines of equivalent depths of 8 and 2000 m for Kelvin waves. Only frequencies lower than 0.4 cpd were used to avoid contamination by wave modes other than Kelvin waves (for example, inertia-gravity waves, or quasi-two-day waves).

Kelvin wave pseudo zonal wind variances for ECMWF analyses are shown in Fig. 4a and for SABER measurements in Fig. 4b. The ECMWF and SABER pseudo zonal wind variances are very similar in the altitude range 21–41 km. This is valid not only for integrated variances but also for single spectral components (Ern et al., 2008). Therefore both altitude-time distributions of pseudo wind variances can serve as references for GROGRAT simulations.

For comparison Fig. 4c shows ECMWF zonal wind variances derived from the original zonal wind data. In the altitude range 20–35 km ECMWF zonal wind spectra and pseudo zonal wind spectra are in good agreement. Therefore also original zonal wind variances and pseudo zonal wind variances (obtained by integrating over the same Kelvin wave band) are almost the same in the altitude range 20–35 km. At higher altitudes the original ECMWF Kelvin wave zonal wind variances are, however, high biased with respect to the pseudo zonal wind variances (this can be over a factor of 2 at 45 km altitude). This hints at some imperfections of the model winds at higher altitudes where few (if any) observational wind data enter the ECMWF operational analyses.

Also at altitudes below the tropopause the original ECMWF Kelvin wave zonal wind variances are much higher than the Kelvin wave pseudo zonal wind variances derived from the temperature spectra. This is likely due to non-Kelvin wave contributions adding additional "noise" in the wind spectra so that we cannot separate the Kelvin wave signal from the overall noise. This confirms our choice to calculate pseudo zonal wind spectra for our simulations because in the temperature spectra Kelvin waves are much more dominant than in the wind spectra and the Kelvin wave signal can be extracted much easier.

Another reason why we choose to use ECMWF temperature spectra for our simulations is that sometimes ECMWF zonal wind spectra contain artifacts. For example, sometimes there are enhanced spectral contributions at zonal wavenumber one, extending over all frequencies from 0–1 cpd. This clearly artificial effect is not seen in the temperature spectra which are therefore believed to be more reliable.

The Kelvin wave pseudo zonal wind variances shown in Fig. 4a and b should therefore be a reliable reference for our simulations with the GROGRAT ray tracer. And since in the stratosphere the ECMWF temperature spectral distribution has been validated by comparison with SABER measurements, we expect the reference distributions shown in Fig. 4a and b to be reproduced, if the GROGRAT source distribution itself is located in the stratosphere – i.e., in the altitude range validated with SABER. In addition, source spectra in the upper troposphere and above are located at altitudes higher than the Kelvin wave source processes, and the

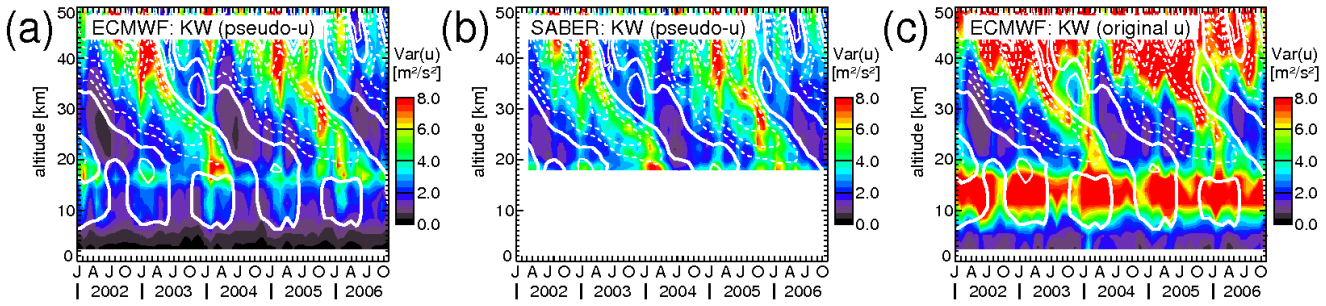

Fig. 4. Altitude-time cross-section of ECMWF **(a)** and SABER **(b)** pseudo zonal wind variances, as well as ECMWF original zonal wind variances **(c)**. All are obtained by integration over the Kelvin wave band between 8 and 2000 m equivalent depth and frequencies <0.4 cpd. The variances shown represent an average over latitudes of 15° S–15° N for ECMWF and 14° S–14° N for SABER (i.e., for SABER the analyses for the latitude bins 0, ±4, ±8, ±12 degrees are averaged). Overplotted contour lines are zonal mean zonal wind from ECMWF averaged over the latitudes 15° S–15° N and the 36-day windows used for the spectral analysis. Contour interval is 10 m/s, solid lines indicate eastward, dashed lines westward wind. The zero wind line is highlighted by a boldface solid line.

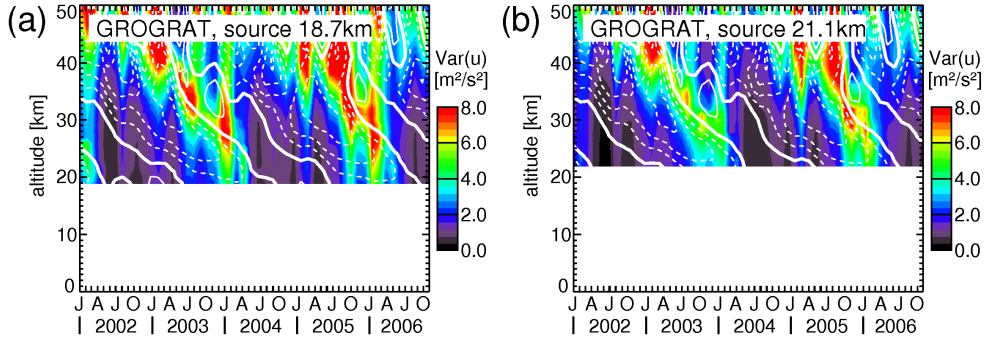

Fig. 5. Altitude-time cross-section of Kelvin wave pseudo zonal wind variances simulated with GROGRAT using time-varying ECMWF source spectra at 18.7 km altitude **(a)** and 21.1 km altitude **(b)**. Again, variances are obtained by integrating over the Kelvin wave band between 8 and 2000 m equivalent depth and frequencies <0.4 cpd. Overplotted contour lines are zonal mean zonal wind from ECMWF averaged over the latitudes 15° S–15° N and the 36-day windows used for the spectral analysis. Contour interval is 10 m/s, solid lines indicate eastward, dashed lines westward wind. The zero wind line is highlighted by a boldface solid line.

complete effect of the forcing should be "contained" in these launch spectra. This will be an important consistency check to find out whether GROGRAT can be applied to Kelvin waves.

For this consistency check we choose source altitudes of 18.7 km and 21.1 km in the lower stratosphere. For comparison the time-averaged ECMWF spectra at 18.7 and 21.1 km altitude are shown in Fig. 2a and b. However, for this consistency check we include temporal variations of the source spectra to be as realistic as possible.

The results of the consistency check are shown in Fig. 5a for 18.7 km, and in Fig. 5b for 21.1 km source altitude. We can see that good agreement is found between the simulated distributions of Kelvin wave variances shown in Fig. 5 and the reference distributions shown in Fig. 4a and b. There are only some minor inconsistencies in the GROGRAT simulations: for example, the decrease of variances due to zonal wind reversals shows a time/altitude lag.

This is further investigated by comparing space-time spectra for a single 36-day time window. Effects of delayed Kelvin wave dissipation are most obvious at altitudes somewhat above the zero wind lines of the wind reversals from QBO easterlies to westerlies. Therefore in Fig. 6 we present spectra for the time window centered on 21 Feb. 2006 at an altitude of 30 km, i.e., about 2 km above the zero wind line. Shown are pseudo zonal wind spectra for SABER and ECMWF (Fig. 6a and b), the original ECMWF zonal wind spectrum (Fig. 6c), and the zonal wind spectrum simulated with GROGRAT (Fig. 6d) based on the simulation with time-varying ECMWF source spectra at a launch altitude of 21.1 km (see Fig. 5b).

Comparison of Fig. 6a and b shows good agreement between SABER and ECMWF also for single pseudo zonal wind spectra. Only due to the contributions of mesoscale gravity waves not resolved by the satellite sampling pattern the spectral background is somewhat higher in the SABER

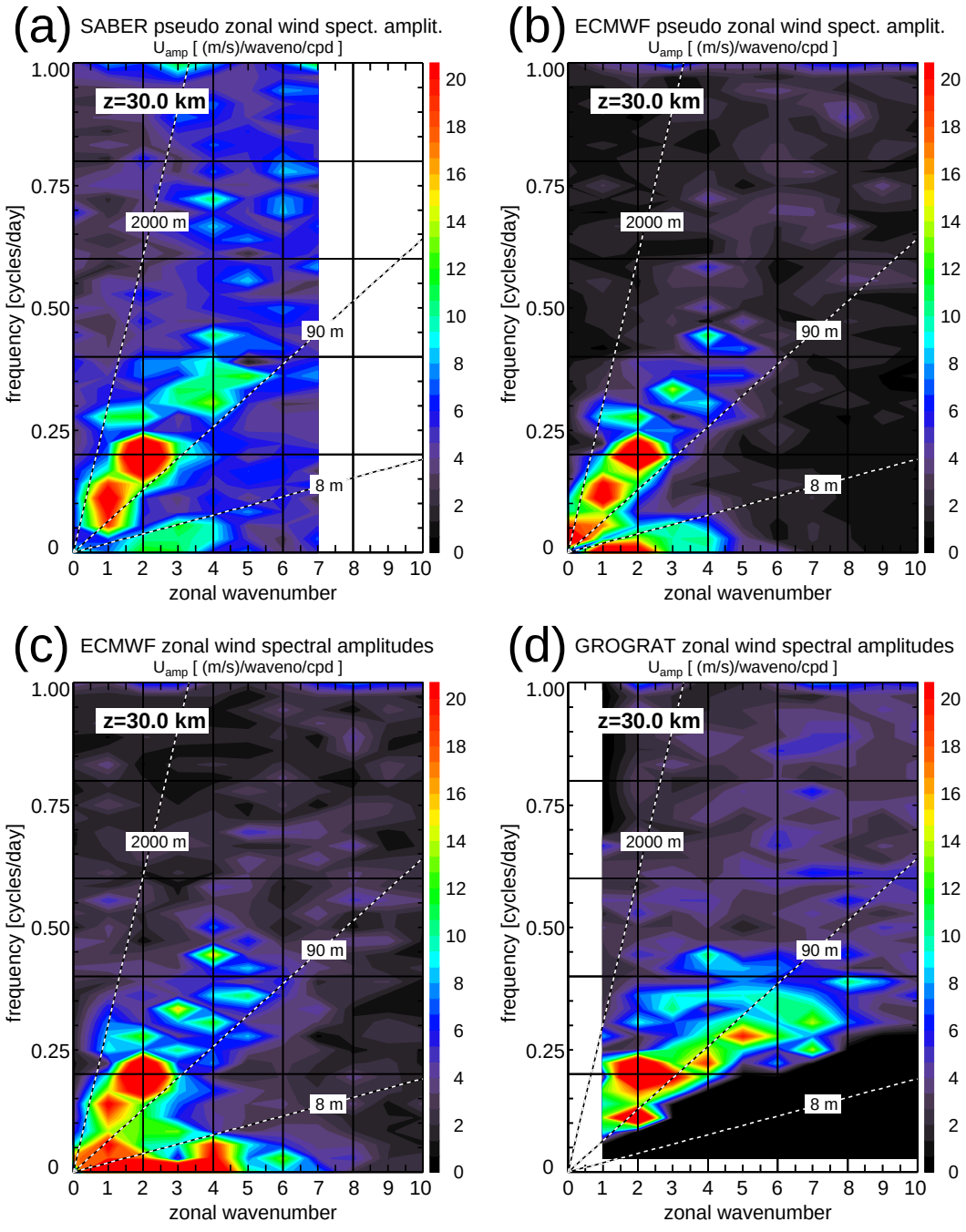

Fig. 6. Zonal wind space-time spectra for the single 36-day time window centered on 21 February 2006 at 30 km altitude. Shown are the spectra for SABER **(a)** and ECMWF **(b)** pseudo zonal wind amplitudes, as well as ECMWF original zonal wind amplitudes **(c)**. Also shown is a zonal wind spectrum simulated with GROGRAT **(d)** based on a simulation with time-varying ECMWF source spectra at a source height of 21.1 km (cf. Fig. 5b).

spectrum. There is also good agreement with the original ECMWF zonal wind spectrum Fig. 6c, indicating that the dispersion relation for Kelvin waves is fulfilled, and indeed the main spectral contributions are due to Kelvin waves. Only at very low ground based phase speeds (below and around the line of 8 m equivalent depth) there are some spectral contributions, which might be due to waves with eastward ground based but westward intrinsic phase speed. (The zonal mean wind is eastward for the spectra shown in Fig. 6.) These contributions however seem not to fulfill the

polarization relations for Kelvin waves and are strongly suppressed in the pseudo zonal wind spectra (Fig. 6a and b), which are derived from temperature spectra. This could, for example be an indication for contributions due to Rossby waves, which usually have only small temperature amplitudes compared to Kelvin waves. These contributions might also be one of the reasons for a high bias of the original ECMWF zonal wind variances (Fig. 4c) with respect to the SABER and ECMWF pseudo zonal wind variances shown in Fig. 4a and b. Even in the altitude range 20–35 km there is some high bias. It should also be noted that all spectra discussed here are symmetric spectra, and the antisymmetric part of the non-Kelvin wave spectral contributions should already be strongly suppressed with respect to "full" spectra containing both symmetric and antisymmetric wave modes.

In Fig. 4a–c the main Kelvin wave contributions are located between the lines of 90 and 2000 m equivalent depth. Slower ground based phase speed Kelvin waves have already dissipated at lower altitudes. Different from this in the simulated GROGRAT spectrum (Fig. 6d) there are still Kelvin wave contributions at lower ground based phase speeds between the lines of 8 and 90 m equivalent depth. This indicates that, indeed, the wave dissipation is somewhat delayed in the GROGRAT simulation.

One reason could be the wave dissipation mechanisms parameterized in GROGRAT, which have not been optimized for the simulation of planetary-scale waves. The delayed wave dissipation could however also be an effect of our very simplified assumptions, using 36-day average launch spectra, averaged over the latitude range from 15° S–15° N, and a background atmosphere which is also averaged over 36 days and latitudes 15° S–15° N. This means that in our simulations zonal and meridional variations in both the source distribution and the atmospheric background are neglected and also inhomogeneities of the global Kelvin wave distribution that might lead to enhanced wave dissipation are not captured.

However, in our current very simplified study we are mainly interested in the first order basic mechanisms governing the global average distribution of Kelvin waves and its interaction with the QBO. Therefore the effects discussed above like, for example, delayed wave dissipation, non-Kelvin wave contributions, or deviations from the global average distribution, will not be further subject of our study because they are minor compared to other effects that are discussed in the following and will have only little effect on the key findings of our study.

4.2 Variation of the source altitude using time-varying ECMWF source spectra

In a next step GROGRAT is employed to simulate altitude-time distributions of Kelvin wave variances using time-varying ECMWF source spectra and source altitudes from 4.9 km up to 18.7 km (troposphere to lower stratosphere). In Fig. 7 the resulting altitude-time distributions of Kelvin wave pseudo zonal wind variances are given for the launch altitudes 4.9 km (a), 8.5 km (b), 11.4 km (c), 13.9 km (d), 16.9 km (e), and 18.7 km (f).

For the two lowest source altitudes 4.9 and 8.5 km (Fig. 7a and b) the variations found in the stratosphere do not exhibit the pronounced band-like structures of the reference distribution which are caused by the QBO. Beneath strong annual and semi-annual variations only weak variation due to the QBO is found. In addition, the variances in the stratosphere are too high. Both findings indicate that these source spectra are only to a minor extent due to freely propagating Kelvin waves and that the amplitudes of these non-Kelvin wave contributions grow considerably over the large altitude range from the troposphere to the stratosphere.

First weak indications of the QBO-induced band-like structures typical for Kelvin waves are found for a launch altitude of 11.4 km (Fig. 7c) and the structures improve more and more the higher we launch. Also the amplitudes found in the stratosphere become more and more realistic.

A general feature in all GROGRAT simulations but especially for the lowest launch altitudes is that at altitudes directly above the source level Kelvin wave variances are lower than in the reference distribution (see Fig. 4). This indicates that part of the variances contained in the source spectra cannot propagate upward and is filtered out directly after launch of the wave component. At low launch altitudes most of the variance contained in the 8–2000 m equivalent depth wave band comes from spectral components with very low ground based phase speeds (see Fig. 1). At these low phase speeds Kelvin waves or gravity waves cannot exist in the given background atmosphere and are therefore not propagated upward.

Provided that the ECMWF spectra represent the "true atmosphere" and are not dominated by noise or artifacts we can conclude from all these results that the altitude region where the Kelvin waves are mainly generated is below about 14 km. The spectra at lower altitudes exhibit mainly seasonal variations and contain spectral noise of "unorganized" convection (not propagating into the stratosphere) rather than coherent signals due to Kelvin waves. This is consistent with the observations by, for example, Randel and Wu (2005) who observed variations due to Kelvin waves down to altitudes of about 12 km in GPS temperatures.

This is further investigated in Fig. 8. In this figure the average relative deviation between the altitude-time distribution of simulated GROGRAT Kelvin wave variances (see Fig. 7) and the reference distributions (see Fig. 4) is plotted as a function of the source altitude. The red (blue) line indicates the average relative deviation between the GROGRAT simulations and the ECMWF (SABER) distribution (Fig. 4a and b) determined in the altitude range 20–50 km. For source altitudes higher than 20 km deviations are determined only between the source altitude and 50 km altitude. For comparison, the purple line also shows the deviations between the GROGRAT simulations and the ECMWF reference distribution (Fig. 4a) in the largest possible altitude range between

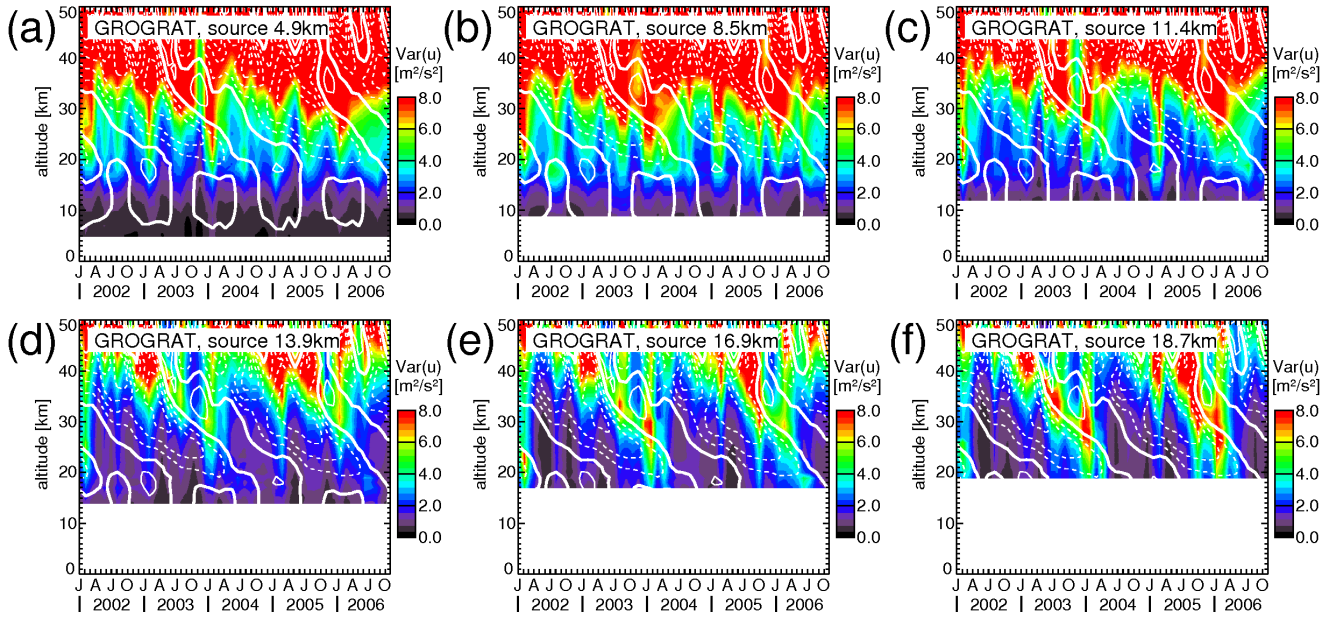

Fig. 7. Altitude-time cross-section of Kelvin wave pseudo zonal wind variances simulated with GROGRAT using time-varying ECMWF source spectra at 4.9 km **(a)**, 8.5 km **(b)**, 11.4 km **(c)**, 13.9 km **(d)**, 16.9 km **(e)**, and 18.7 km altitude **(f)**. Again, variances are obtained by integrating over the Kelvin wave band between 8 and 2000 m equivalent depth and frequencies <0.4 cpd. Overplotted contour lines are zonal mean zonal wind from ECMWF averaged over the latitudes 15° S–15° N and the 36-day windows used for the spectral analysis. Contour interval is 10 m/s, solid lines indicate eastward, dashed lines westward wind. The zero wind line is highlighted by a boldface solid line.

the source altitude and 50 km altitude. The green dashed vertical line indicates the average relative deviation between the two reference distributions (Fig. 4a and b) determined in the altitude region 18–50 km.

In all cases deviations are high for the lowest launch altitudes of 4.9 and 8.5 km and drop sharply in the altitude range 8.5–13.9 km. Above 14 km only minor improvements are achieved.

The fact that the average relative deviations between GROGRAT simulations and ECMWF reference are somewhat lower for the lowest launch altitudes if a larger altitude interval is taken to determine the deviations (purple line in Fig. 8) indicates that there is a severe high-bias of the variances at high altitudes if low source levels are chosen. This high-bias is somewhat mitigated if also lower altitudes with lower deviations are considered for the calculation of the average relative deviations (see Fig. 7).

It should be noted that the deviation from the SABER reference is generally somewhat larger because the SABER spectra contain a spectral background due to small scale gravity waves not resolved by the satellite sampling. This background is strongly reduced in the ECMWF spectra and therefore also not contained in the ECMWF source spectra. Of course, this kind of background cannot be reproduced by our GROGRAT simulations requiring that all spectral components of the source spectrum are properly resolved by the sampling (or model grid in the case of ECMWF data), so that zonal wavenumber and phase speed can directly be determined from the space-time spectrum.

It should also be stated clearly that the method used to determine the minimum altitude where freely propagating Kelvin waves dominate the spectra is strongly dependent on the parameter analyzed. For example, if we would have analyzed original ECMWF zonal wind data we would have obtained a higher altitude than for pseudo zonal winds, simply because Kelvin waves can be better identified in pseudo zonal wind spectra than in original zonal wind spectra. This is the case because pseudo zonal wind spectra are derived from temperature spectra, where Kelvin waves are much more dominant. And there may be parameters that are even better suited for the identification of Kelvin waves than temperatures.

Our method fails to extract the Kelvin wave signal below about 14 km altitude. However, more sophisticated methods might also be able to identify Kelvin wave signals at even lower altitudes. In addition, some bias could be introduced by neglecting horizontal variations in the source spectra and zonal background wind. Therefore our value of 14 km altitude where freely propagating Kelvin waves on global average start to dominate the space-time spectra is only some kind of upper limit to this value.

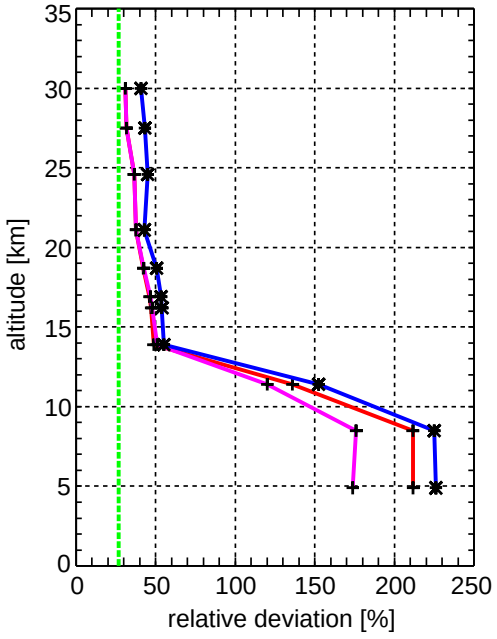

Fig. 8. Average relative deviation between the altitude-time distribution of simulated GROGRAT Kelvin wave variances and the ECMWF and SABER reference distributions for different source altitudes. Blue line: deviation between GROGRAT and SABER determined in the altitude range 20–50 km, red line: deviation between GROGRAT and ECMWF determined in the altitude range 20–50 km, purple line: deviation between GROGRAT and ECMWF determined in the altitude range between source altitude and 50 km, green line: average relative deviation between the SABER and ECMWF reference distributions.

4.3 Variation of the source altitude using time-averaged ECMWF source spectra

In the following we want to investigate whether the QBO-related variation of Kelvin wave variances observed in the stratosphere is only an effect of the interaction of the Kelvin waves with the QBO wind system and its alternating zonal wind directions, or if also temporal variations of the source processes play an important role. For this purpose Kelvin wave variances are simulated with GROGRAT like in Sect. 4.2 but with constant (time-averaged over the period January 2002–November 2006) ECMWF source spectra (see Fig. 1). Again, we use the same source altitudes from 4.9–18.7 km. These source spectra at different altitudes contain the shift of the lobe-shaped spectral peak due to Kelvin waves with altitude but no seasonal variations of this shift and of the amplitudes.

The results are similar to those obtained with time varying source spectra (see Fig. 9). This indicates that large part of the variations seen in the stratosphere is caused by modulation of the variances due to background wind variations. Even the QBO-related band-like structures evolve if we launch at higher altitudes (11.4–18.7 km).

However, large part of the seasonal variations also found in the variances (annual, semi-annual) are smoothed out. In addition, the band-like QBO structures observed in the stratosphere start with much too low amplitudes in the lower stratosphere. This is most likely caused by using an average amplitude which is too low during the QBO easterly periods in the upper troposphere/lower stratosphere (UTLS).

This means: if we want to obtain all variations observed in the stratosphere seasonal variations of the source spectrum are required. In Sect. 5 an attempt will be made to use seasonal variations directly from measurements of the Tropical Rainfall Measuring Mission (TRMM) satellite (OLR and rain rates) instead of modeled ECMWF spectra.

5 OLR and rainfall spectra as source distributions for ray tracing simulations

In this section we will use space-time spectra of outgoing longwave radiation (OLR) as well as spectra of rain rates from the Precipitation Radar (PR) and the TRMM Microwave Imager (TMI) sensors onboard the TRMM satellite as source distribution for our GROGRAT simulations. An overview of the PR and TMI measurements is, for example, given in Stephens and Kummerow (2007). The OLR and rain rate source distributions have the advantage that the variability of measured data at the source level is directly contained in the source spectra.

Of course, TOVS/ATOVS infrared radiance data (Li et al., 2000) and since 28 June 2005 also rain affected SSM/I microwave radiances (Bauer et al., 2006a,b; Lopez, 2007) are assimilated in the ECMWF operational analyses we use. So the raw measured OLR spectra are not necessarily a better source distribution than ECMWF spectra because the ECMWF spectra should contain already information from OLR measurements.

Also part of the rain rate information should be contained in the ECMWF analyses, however the assimilation of rainfall data is still in progress (Benedetti et al., 2005; Lopez, 2007) and TMI data are assimilated in the ECMWF analyses not earlier than November 2007, this means only after the time period considered in our analyses. Therefore there still might be some benefit using measured TRMM rain rate spectra. In addition, our analyses can provide further information whether the use of raw rain rate and OLR measurements as proxies for latent heat release and deep convection in the tropics is justified.

We do not expect that OLR or rain rate spectra have exactly the same spectral shape as the zonal wind spectra discussed in the previous sections. One reason is that OLR and rain rate spectra represent an altitude range while the zonal wind spectra are given for fixed altitudes. Another reason is that both OLR and rain rates are directly coupled with the latent heat release acting as source mechanism for Kelvin and other equatorial waves. In a theoretical framework the

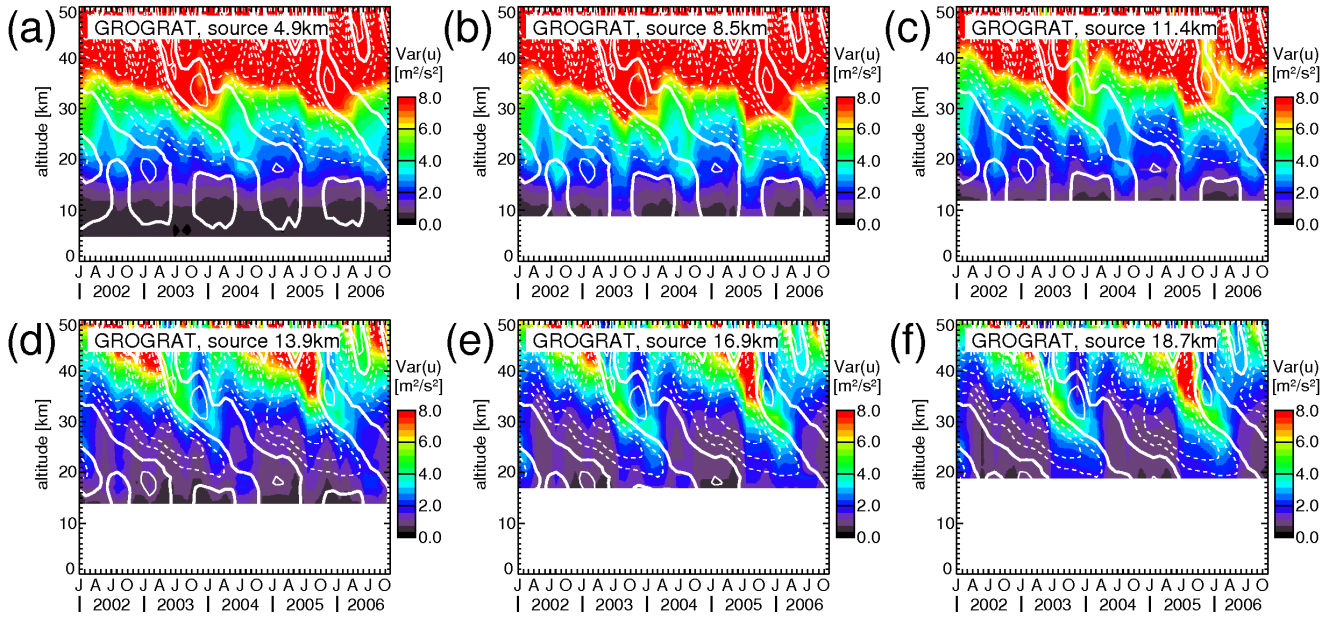

Fig. 9. Altitude-time cross-section of Kelvin wave pseudo zonal wind variances simulated with GROGRAT using time-independent ECMWF source spectra averaged over the period January 2002–November 2006 at the source altitudes 4.9 km **(a)**, 8.5 km **(b)**, 11.4 km **(c)**, 13.9 km **(d)**, 16.9 km **(e)**, and 18.7 km **(f)** (see also Fig. 1). Again, variances are obtained by integrating over the Kelvin wave band between 8 and 2000 m equivalent depth and frequencies <0.4 cpd. Overplotted contour lines are zonal mean zonal wind from ECMWF averaged over the latitudes 15° S–15° N and the 36-day windows used for the spectral analysis. Contour interval is 10 m/s, solid lines indicate eastward, dashed lines westward wind. The zero wind line is highlighted by a boldface solid line.

dynamic response of the atmosphere (e.g., geopotential, temperature or wind spectra) in the near field (just above the top of the convective source) is usually obtained by projecting this spectrum on a set of Hough modes representing the wave modes that are able to propagate vertically in the atmosphere (e.g., Salby and Garcia, 1987; Bergman and Salby, 1994; Ricciardulli and Garcia, 2000). In doing so the spectral shape is changed. In particular, the red nature of the heating spectra is reduced by filtering out low frequency contributions (at equivalent depths lower than about 8 m) that cannot propagate due to their short vertical wavelengths (Bergman and Salby, 1994; Ricciardulli and Garcia, 2000).

On the other hand we have seen in Sect. 4.3 that large part of the variation of Kelvin wave variances can be explained by a combination of the effect of the QBO winds and seasonal variations of the source spectrum. Therefore more realistic seasonal variations in the OLR and rain rate spectra might overcompensate the somewhat different spectral shapes. Especially, because we use only equivalent depths larger than 8 m for determining the Kelvin wave variances (see above). In this way part of the low frequency contributions not belonging to propagating wave modes in the OLR and rain rate spectra will not contribute to the variances we determine.

It has been shown by Kubar and Hartmann (2008) that the cloud tops of heavy precipitating clouds are mainly located at altitudes between about 11 and 17 km in the western and eastern Pacific. Also in airborne remote sensing data in the tropics an opaque cloud cover is often found at altitudes below about 14–17 km (e.g., Spang et al., 2008). This altitude range is in good agreement with the altitude of about 14 km which was found to be the top of the source altitude region on global average (see Sect. 4.2). At altitudes above about 14 km most of the spectral information of the source processes is contained in the space-time spectra, and at these higher altitudes wave filtering due to the background atmosphere will dominate over wave generation by latent heat release. This means that the altitude range of 14 km and several kilometers above should be best suited as launch altitudes for GROGRAT simulations based on OLR and rain rate spectra.

The space-time spectra from TRMM OLR and rain rates were determined for frequencies lower than 0.5 cpd in 96-day time windows using a time step of 36 days (Cho et al., 2004) with the center days exactly corresponding to the 36-day windows used before. In our analysis we again use only symmetric spectra with frequencies >0 (= eastward) averaged over the latitude range 15° S–15° N.

Average spectra (averaged over the period January 2002–November 2006) are shown in Fig. 10. The spectral shape is similar to the ECMWF spectra for 11.4 and 13.9 km altitude in Fig. 1 with the spectral contribution of Kelvin waves showing up between the lines of 8 and 90 m equivalent depth. However, the spectra shown in Fig. 10 are more "red" than

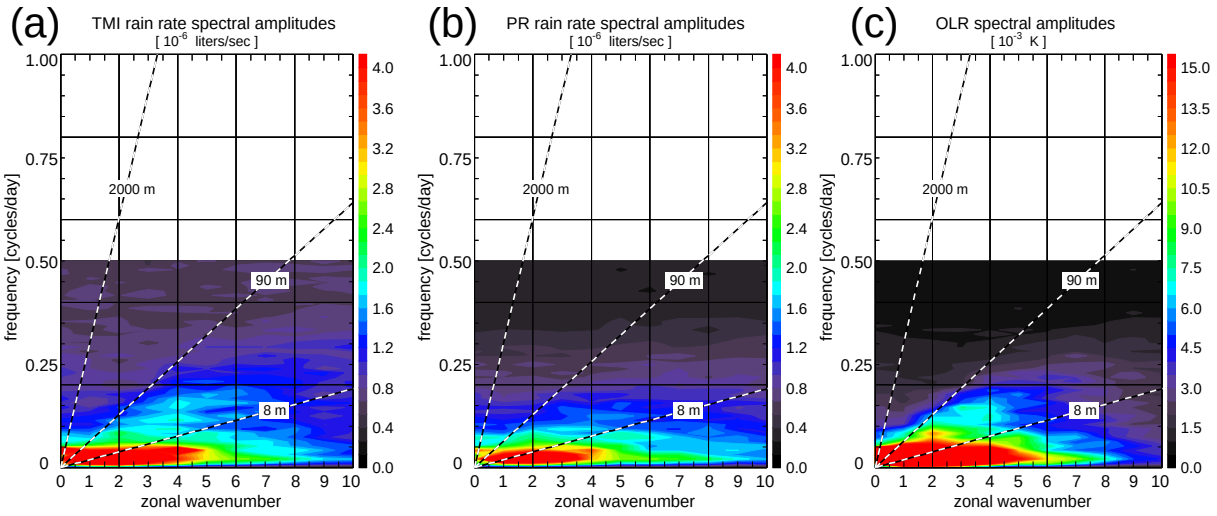

Fig. 10. TRMM spectral amplitudes averaged over the period January 2002–November 2006 for TMI rain rates **(a)**, PR rain rates **(b)**, and OLR **(c)**. Also given are the lines for equivalent depths h_e=8, 90, and 2000 m, corresponding to ground based phase speeds of 9, 30, and 140 m/s.

the ECMWF spectra in Fig. 1 with strong spectral contributions at low frequencies even at high zonal wavenumbers. Maybe this is due to the fact that the TRMM spectra cannot be attributed to a single fixed altitude but represent spectral contributions of a "mixture" of altitudes, containing also contributions of very low altitudes.

As before, we need zonal wind spectra as input for the GROGRAT ray tracer. Two methods for estimating zonal wind spectra from rain rate spectra as well as OLR spectra are discussed in the following subsections.

5.1 Constant scaling factor for TRMM spectra derived from ECMWF spectra

For the first method we assume that the average pseudo zonal wind amplitudes derived from the ECMWF spectra used in Sect. 4.3 are realistic and can serve as a basis to derive a fixed scaling factor for obtaining pseudo zonal wind spectra from TRMM rain rate and OLR spectra. This fixed scaling factor is determined separately for each of the fixed ECMWF pressure altitudes under the assumption that average pseudo wind variances have to be equal for both TRMM and ECMWF spectra in the zonal wavenumber range 1–6 and between the lines of 8 and 2000 m equivalent depth and frequencies $<$0.4 cpd. This is exactly the range used to determine Kelvin wave variances in our analyses.

The scaling of the spectral amplitudes is carried out as follows:

$$\hat{\Psi}_{\mathrm{TR,sc}}(k,\omega;t;z_s) = \hat{\Psi}_{\mathrm{TR}}(k,\omega;t) \times \left[\frac{\int_{k,\omega} \hat{\Psi}^2_{\mathrm{EC,av}}(k,\omega;z_s) d\omega dk}{\int_{k,\omega} \hat{\Psi}^2_{\mathrm{TR,av}}(k,\omega) d\omega dk} \right]^{1/2} \quad (8)$$

with $\hat{\Psi}_{\mathrm{TR,sc}}(k,\omega;t;z_s)$ the time-varying pseudo zonal wind spectral amplitudes which will be used in our analysis, $\hat{\Psi}_{\mathrm{TR}}(k,\omega;t)$ the time-varying TRMM rain rate or OLR spectral amplitudes, $\hat{\Psi}_{\mathrm{TR,av}}(k,\omega)$ the time-averaged TRMM rain rate or OLR spectral amplitudes, and $\hat{\Psi}_{\mathrm{EC,av}}(k,\omega;z_s)$ the time-averaged ECMWF pseudo zonal wind spectral amplitudes (see Eq. 7) at a specified source altitude z_s. The integral $\int_{k,\omega} \ldots d\omega dk$ indicates the integration over the zonal wavenumber range 1–6 between the lines of 8 and 2000 m equivalent depth for frequencies $<$0.4 cpd.

This method has the advantage that both spectral shape and temporal variations of the TRMM spectra are conserved. However, the fact that the TRMM spectra are too red compared with the ECMWF spectra causes a low-bias in the Kelvin wave band at higher altitudes because low frequencies are more and more dissipated with increasing altitude and too low amplitudes are launched at higher frequencies. In addition, the QBO-related bands of high Kelvin wave variances are only weakly indicated.

This becomes obvious in Fig. 11 showing the altitude-time distribution of Kelvin wave pseudo zonal wind variances resulting from GROGRAT simulations with the time-varying TMI source spectrum launched at the set of different source altitudes used before. Again, we find that the higher source altitudes perform best in reproducing the temporal variations of the reference distributions. However, we find the low-bias of variances mentioned above, the more the higher we launch. At low source altitudes the spectral shapes of TMI and the ECMWF spectrum at these altitudes are still similar and the scaling factor derived from the average spectra is still realistic. At higher source altitudes, however, the TMI spectrum is too red compared with the ECMWF source spectrum and there are too strong spectral contributions at low

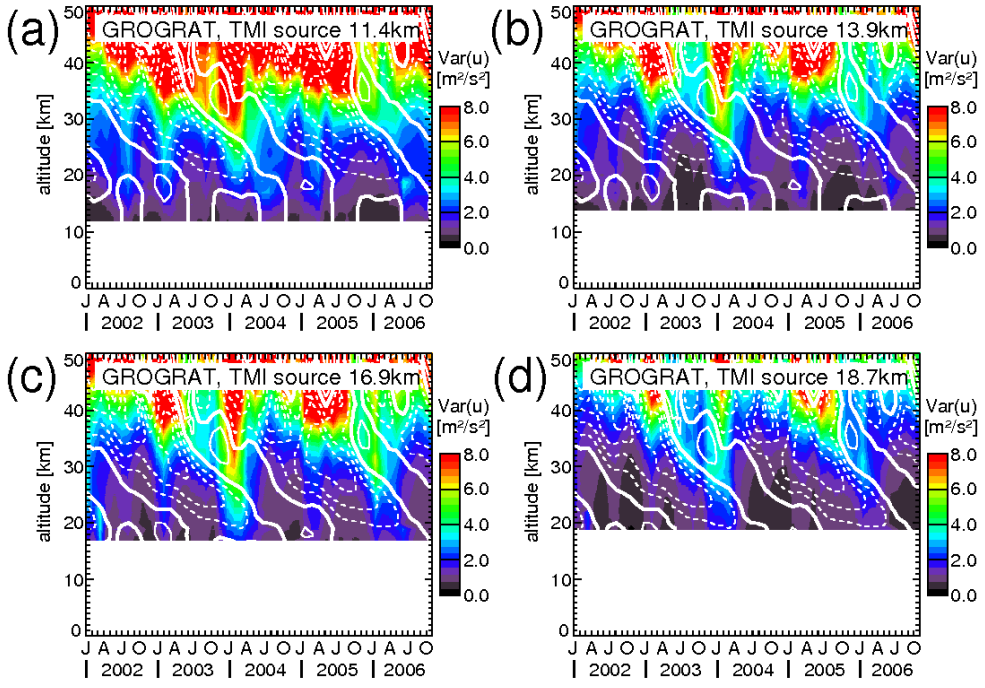

Fig. 11. Altitude-time cross-section of Kelvin wave pseudo zonal wind variances simulated with GROGRAT using time-varying TRMM-TMI source spectra normalized with time-averaged ECMWF source spectra at the source altitudes 11.4 km **(a)**, 13.9 km **(b)**, 16.9 km **(c)**, and 18.7 km **(d)**. Again, variances are obtained by integrating over the Kelvin wave band between 8 and 2000 m equivalent depth and frequencies <0.4 cpd. Overplotted contour lines are zonal mean zonal wind from ECMWF averaged over the latitudes 15° S–15° N and the 36-day windows used for the spectral analysis. Contour interval is 10 m/s, solid lines indicate eastward, dashed lines westward wind. The zero wind line is highlighted by a boldface solid line.

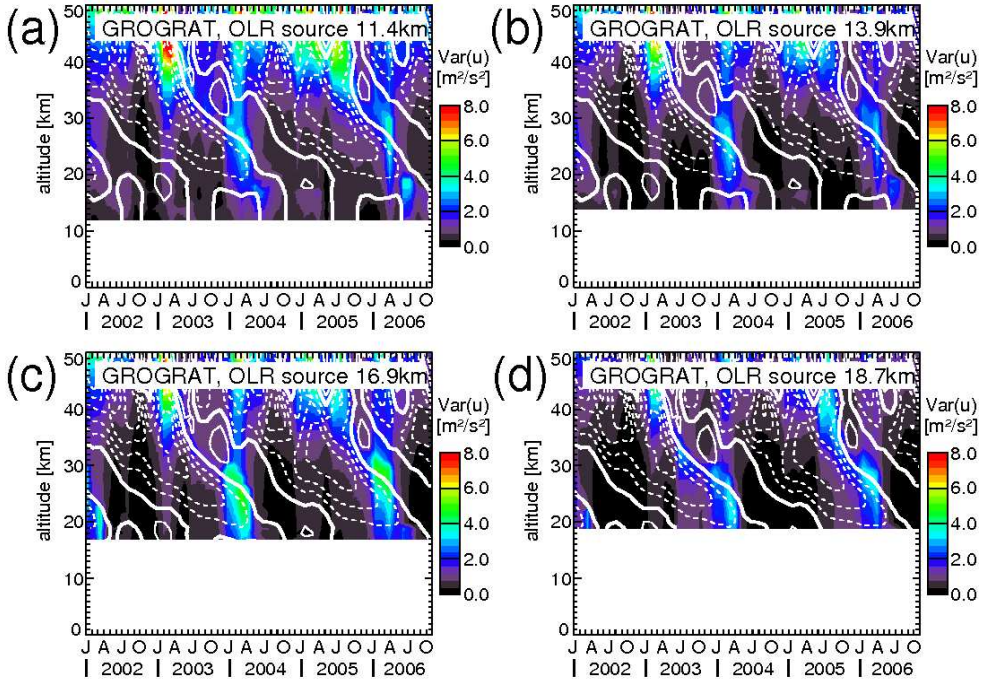

Fig. 12. Same as Fig. 11 but for GROGRAT using normalized time-varying TRMM-OLR source spectra.

frequencies, and these low phase speed components in the TMI source spectrum are filtered out because they dissipate and cannot propagate upward.

The results are similar for PR rain rates (not shown) but even worse for OLR source spectra (Fig. 12) because the OLR spectra are even more dominated by low phase speed spectral components.

This indicates that the role of the spectral shape is too important, and the approach chosen is too simple. Maybe the more sophisticated approach of projecting the OLR or rain rate spectra on Hough modes would perform better but this will not be subject of our study. Therefore, we will follow another simple approach in the next subsection.

5.2 Average ECMWF spectra with seasonal variations taken from TRMM measurements

Because for none of the source altitudes the reference distributions can be reproduced satisfactorily we will now avoid the contamination of the launch spectra by low phase speed wave components. We assume that, although noise due to unorganized convection in the TRMM spectra or maybe also effects of the Madden Julian Oscillation (MJO) at low phase speeds might cause problems to derive a constant scaling factor, the measured temporal variations of the TRMM spectra could be more realistic than the variations of the ECMWF spectra.

Therefore for the basic shape of the launch spectrum we adopt the time-averaged ECMWF source spectra used in Sect. 4.3, while temporal variations of the source distribution are taken from TRMM measurements. For this purpose relative temporal variations of the TRMM spectra with respect to the time-averaged TRMM spectra as a reference (see Fig. 10) are determined. This means the average spectral shape is taken from ECMWF and the relative variations of the source spectra are taken from TRMM rain rate or OLR spectra spectral component by spectral component.

The scaling of the average ECMWF spectral amplitudes with the measured seasonal variations is carried out as follows:

$$\hat{\Psi}_{\mathrm{TR,rel}}(k,\omega;t;z_s) = \hat{\Psi}_{\mathrm{EC,av}}(k,\omega;z_s)\left[\frac{\hat{\Psi}_{\mathrm{TR}}(k,\omega;t)}{\hat{\Psi}_{\mathrm{TR,av}}(k,\omega)}\right] \quad (9)$$

with $\hat{\Psi}_{\mathrm{TR,rel}}(k,\omega;t;z_s)$ the time-varying pseudo zonal wind spectral amplitudes which will be used in our analysis, $\hat{\Psi}_{\mathrm{TR}}(k,\omega;t)$ the time-varying TRMM rain rate or OLR spectral amplitudes, $\hat{\Psi}_{\mathrm{TR,av}}(k,\omega)$ the time-averaged TRMM rain rate or OLR spectral amplitudes, and $\hat{\Psi}_{\mathrm{EC,av}}(k,\omega;z_s)$ the time-averaged ECMWF pseudo zonal wind spectral amplitudes (see Eq. 7) at a specified source altitude z_s.

By treating each spectral component separately we take into account that seasonal variations can be different for different zonal wavenumbers and frequencies. In addition, the problem that there is no well-defined source altitude for the rain rate and OLR spectra should be reduced.

The results are shown in Fig. 13 for TMI rain rates. We find that now the variances are higher than before and especially for high source altitudes the results look more realistic. Again, the variance distribution is similar for PR source spectra (Fig. 14). For OLR source spectra (Fig. 15) the seasonal variations are more pronounced than in the TMI and PR data. But there is good agreement between all three TRMM source distributions and the ECMWF and SABER reference distributions (see Fig. 4).

In the tropics precipitation is strongly linked with deep convection and, consequently, also with the occurrence of high clouds. Therefore observations of OLR are often used for indirect estimates of precipitation and latent heat release (Arkin and Ardanuy, 1989; Hendon and Woodberry, 1993). The above results show that, indeed, rain rate as well as OLR spectra can serve as source distribution for Kelvin wave simulations. This is a further confirmation that both rain rate and OLR data are good proxies for the total heat released in the tropospheric column, i.e. the source process for Kelvin waves in the equatorial region.

6 Summary and conclusions

In our study we present a novel approach of combining space-time spectral analysis of measured data as well as ECMWF operational analyses with ray tracing techniques. Latitudinally averaged (15° S–15° N) longitude-time spectra resulting from a windowed space-time Fourier analysis using non-overlapping 36-day time windows of ECMWF pseudo zonal wind variances were used as input (various source levels from 4.9–30.0 km altitude) for the GROGRAT ray tracing model. This approach allowed to simulate the propagation of equatorial Kelvin waves with the GROGRAT model, although originally developed for ray tracing of gravity waves. Rays are launched eastward for each of the independent spectral grid points of a space-time spectrum at a given source level. Only vertical propagation of the rays is considered.

The space-time spectra used as source distribution represent global averages over 36-days and the latitude range 15° S–15° N. Based on these spectra our results address some global aspects of the generation and propagation of Kelvin waves. For our investigations space-time spectra and altitude-time distributions of Kelvin wave variances from ECMWF analyses as well as from SABER measurements are taken as reference.

It was found that mainly radiative wave damping is responsible for the shift of the Kelvin wave spectral peak towards higher phase speeds with increasing altitude. Turbulent damping plays only a minor role, and the amplitude limit critical for wave breaking is never reached in our simulations. The process responsible for the shift of the Kelvin wave spectral peak has been introduced as "differential radiative damping" for the first time by Garcia and Salby (1987).

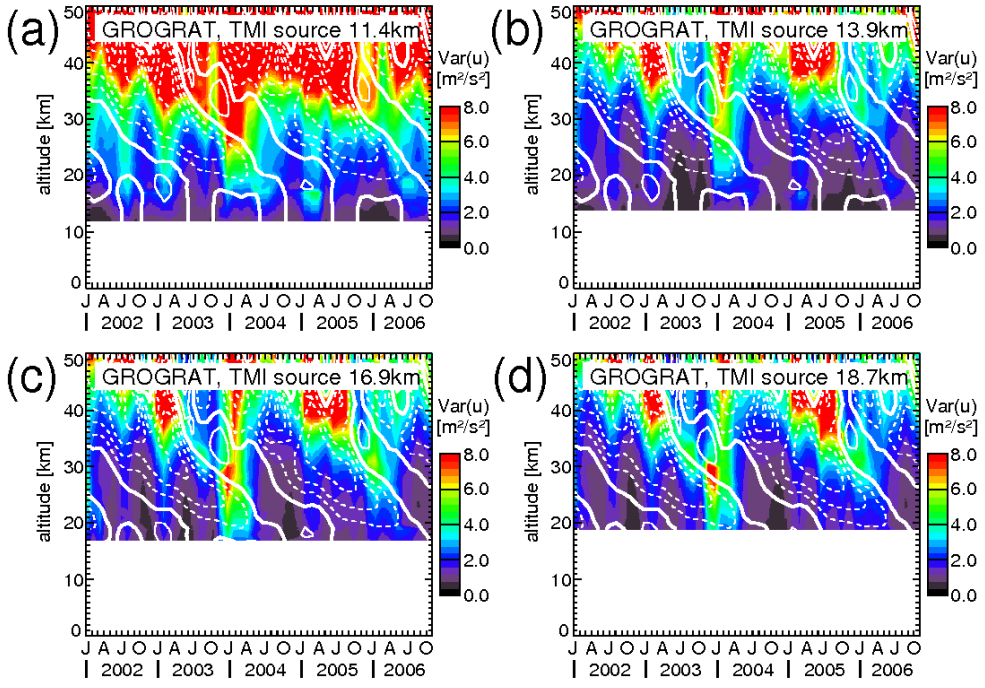

Fig. 13. Altitude-time cross-section of Kelvin wave pseudo zonal wind variances simulated with GROGRAT using seasonal variations from TRMM-TMI and the time-averaged spectral shape of ECMWF source spectra at the source altitudes 11.4 km **(a)**, 13.9 km **(b)**, 16.9 km **(c)**, and 18.7 km **(d)**. Again, variances are obtained by integrating over the Kelvin wave band between 8 and 2000 m equivalent depth and frequencies <0.4 cpd. Overplotted contour lines are zonal mean zonal wind from ECMWF averaged over the latitudes 15° S–15° N and the 36-day windows used for the spectral analysis. Contour interval is 10 m/s, solid lines indicate eastward, dashed lines westward wind. The zero wind line is highlighted by a boldface solid line.

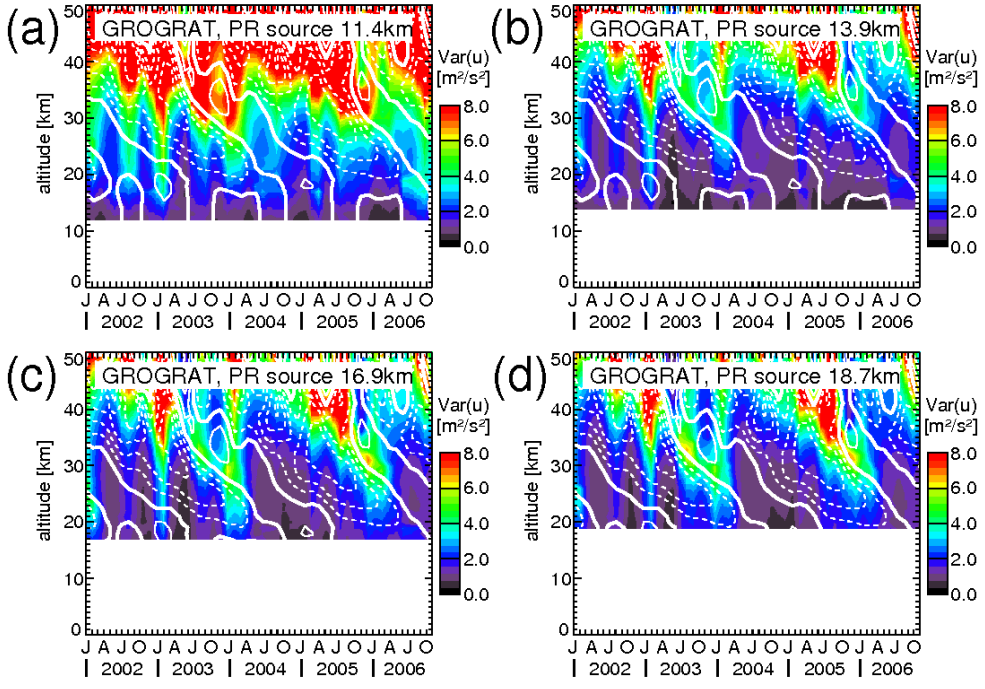

Fig. 14. Same as Fig. 13 but for seasonal variations taken from TRMM-PR measurements.

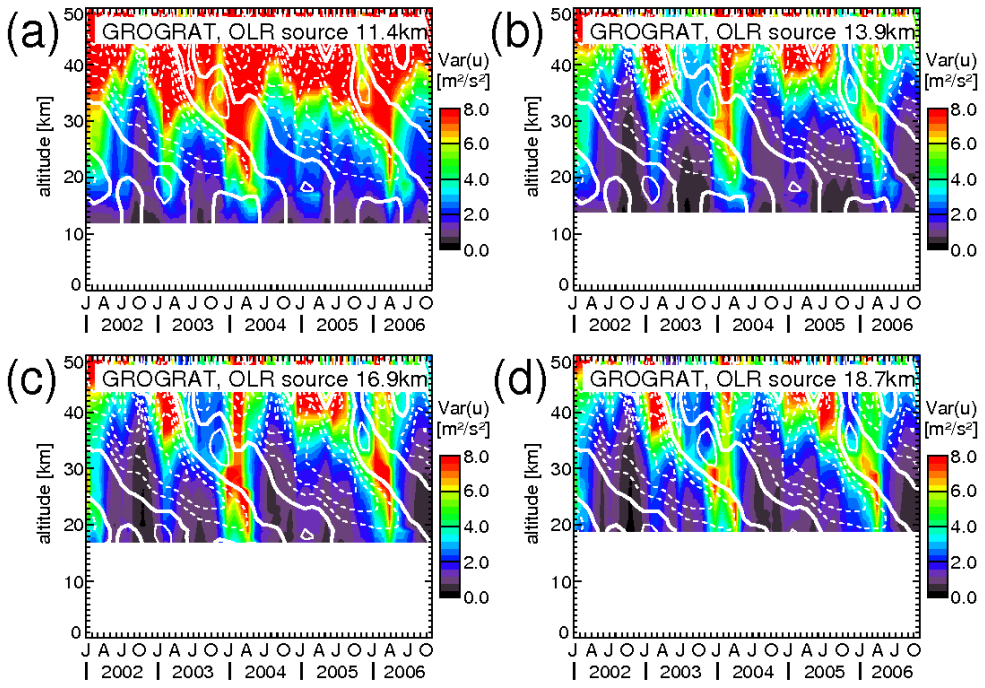

Fig. 15. Same as Fig. 13 but for seasonal variations taken from TRMM-OLR measurements.

Vertical and temporal variations of Kelvin wave variances can be reproduced if source distributions are located in the stratosphere (at altitudes above all source processes), indicating that the GROGRAT ray tracer indeed can simulate the basic properties of Kelvin waves.

Variation of the source altitude in the GROGRAT simulations reveals that the stratospheric distribution of Kelvin wave variances can only be reproduced if the source altitudes are located above about 14 km. At lower source altitudes the frequency distribution of the ECMWF source spectra is too red, indicating that part of the spectral contributions at low altitudes is "noise" due to unorganized tropospheric convective activity and not due to waves that can propagate vertically. From these findings we can conclude that the bulk of the Kelvin wave source processes (latent heat release due to deep convection) is located at altitudes below 14 km on global average. It should however be noted that this value is only some kind of upper limit to this altitude.

Part of the distribution of Kelvin wave variances can already be reproduced using a constant average source spectrum. This is the case because already the interaction of the launched waves with the background wind field causes a QBO-related variation of the wave variances. Nevertheless, it turns out that seasonal variations of the source spectra are very important to explain all of the variation of wave variances observed.

We further investigated whether space-time spectra determined from TRMM satellite measurements (OLR and rain rates from the TMI and PR sensors) can be used as source distributions. However, simple scaling of the OLR and rain rate spectra to obtain the same variances in the Kelvin wave band as in ECMWF spectra for a specified source altitude leads to a low bias in stratospheric wave variances because the launch spectra are too red.

Another approach was made, using the spectral shape of the average ECMWF source spectra at the selected source altitude and the seasonal variations from the OLR and rain rate spectra, independently for each single spectral component. This approach performs much better, and the results are similar to the ones obtained before with ECMWF source spectra. While seasonal variations in the rain rate spectra are a bit too weak, results obtained from OLR source spectra show slightly too strong annual variations. Nevertheless, all three TRMM source distributions perform well and show good agreement with the ECMWF and SABER reference distributions. This confirms the suitability of both rain rate and OLR data as good proxies for deep convection and latent heat release in the tropics.

Appendix A

Derivation of Kelvin wave zonal wind amplitudes from temperature amplitudes

Kelvin wave pseudo zonal wind amplitudes are obtained by using the polarization relations given in Fritts and Alexander

(2003) and Ern et al. (2004), which are valid for a general linear wave approach.

We start from Eqs. (15) and (18) in Fritts and Alexander (2003):

$$-i\hat{\omega}\tilde{u} - f\tilde{v} + ik\tilde{p} = 0 \quad \text{(A1)}$$

$$-i\hat{\omega}\tilde{\Theta} + (N^2/g)\tilde{w} = 0 \quad \text{(A2)}$$

Here $\hat{\omega}$ is the intrinsic frequency, $\tilde{u}$, $\tilde{v}$ and $\tilde{w}$ are the zonal, meridional and vertical wind amplitudes of the wave, k the zonal wavenumber, $\tilde{p}$ the pressure amplitude divided by the atmospheric background density ($p'/\bar{\rho}$), $\tilde{\Theta}$ the relative potential temperature amplitude (Θ'/Θ), N the buoyancy frequency, f the Coriolis frequency, and g the gravity acceleration.

In addition we make use of Eq. (A7) in Ern et al. (2004):

$$\tilde{w} = \frac{-\hat{\omega}}{N^2 - \hat{\omega}^2}\left(m + i\left(\frac{1}{2H} - \frac{g}{c_s^2}\right)\right)\tilde{p} \quad \text{(A3)}$$

Here m is the vertical wavenumber, H the pressure scale height, and c_s the sound speed.

For Kelvin waves the meridional wind amplitude $\tilde{v}$ in Eq. (A1) is zero. By combining Eqs. (A1), (A2) and (A3), replacing $\tilde{w}$ and $\tilde{p}$, we obtain the polarization relation between $\tilde{\Theta}$ and $\tilde{u}$, which can be written as follows:

$$\tilde{\Theta} = \frac{i}{g}\,\frac{1}{1 - \hat{\omega}^2/N^2}\left[m + i\left(\frac{1}{2H} - \frac{g}{c_s^2}\right)\right]\frac{\hat{\omega}}{k}\tilde{u} \quad \text{(A4)}$$

Since:

$$\left|\frac{1}{2H} - \frac{g}{c_s^2}\right| \ll m = \frac{2\pi}{\lambda_z} \quad \text{(A5)}$$

for vertical wavelengths λ_z<50 km, and we can also assume that $\hat{\omega}^2 \ll N^2$, this equation can be further simplified:

$$\tilde{\Theta} = \frac{i}{g}\,m\,\frac{\hat{\omega}}{k}\tilde{u} \quad \text{(A6)}$$

indicating a 90° phase shift between zonal wind perturbation and potential temperature perturbation for Kelvin waves.

We further assume that all motions are adiabatic. The potential temperature is defined as follows:

$$\Theta = T\,(p_0/p)^{\kappa} \quad \text{(A7)}$$

Here p_0 is the reference (surface) pressure and $\kappa = 1 - 1/\gamma$ with γ the adiabatic coefficient:

$$\gamma = c_p/c_v \quad \text{(A8)}$$

which is the ratio of the specific heats for constant pressure and constant volume. For diatomic gases like air: γ=1.4.

From Eq. (A7) we obtain the relationship between relative potential temperature amplitude $\tilde{\Theta}$, relative temperature amplitude $\tilde{T} = T'/T$ and relative pressure amplitude $\tilde{p} = p'/\bar{\rho}$:

$$\tilde{\Theta} = \tilde{T} - \frac{\gamma - 1}{c_s^2}\tilde{p} \quad \text{(A9)}$$

and together with Eq. (A1), assuming $\tilde{v}$=0 for Kelvin waves, $\tilde{p}$ can be eliminated:

$$\tilde{\Theta} = \tilde{T} - \frac{\gamma - 1}{c_s^2}\frac{\hat{\omega}}{k}\tilde{u} \quad \text{(A10)}$$

By combining Eqs. (A10) and (A6) we obtain the polarization relation between temperature perturbation and zonal wind perturbation:

$$\tilde{T} = \left[\frac{\gamma - 1}{c_s^2} + \frac{i}{g}m\right]\frac{\hat{\omega}}{k}\tilde{u} \quad \text{(A11)}$$

The term $(\gamma - 1)/c_s^2$ can be neglected for short vertical wavelengths λ_z<20 km, giving the simple equation:

$$\tilde{T} = \frac{i}{g}\,m\,\frac{\hat{\omega}}{k}\tilde{u} \quad \text{(A12)}$$

Together with the dispersion relation for Kelvin waves (Eq. 1) $\hat{\omega}/k = -N/m$ we obtain the following very simple equation for estimating zonal wind amplitudes $\tilde{u}$ from given temperature amplitudes T':

$$|\tilde{u}| \approx \frac{g}{N}|\tilde{T}| = \frac{g}{N}\frac{|T'|}{T} \quad \text{(A13)}$$

However, because in our simulations vertical wavelengths up to about 50 km or even longer are considered (corresponding to equivalent depths of about h_e=2000 m), we use the following more complete equation obtained by combining Eqs. (A10) and (A4) and assuming $\hat{\omega}^2 \ll N^2$ for calculating zonal wind amplitudes from temperature amplitudes:

$$|\tilde{u}| = \left|\frac{k}{\hat{\omega}}\right|\frac{|T'|}{T}\Bigg/\sqrt{\left[\frac{\gamma - 1}{c_s^2} - \frac{1}{g}\left(\frac{1}{2H} - \frac{g}{c_s^2}\right)\right]^2 + \left[\frac{m}{g}\right]^2} \quad \text{(A14)}$$

or further simplified and m replaced via the dispersion relation for Kelvin waves $\hat{\omega}/k = -N/m$ (Eq. 1):

$$|\tilde{u}| = \left|\frac{k}{\hat{\omega}}\right|\frac{|T'|}{T}\Bigg/\sqrt{\left[\frac{\gamma}{c_s^2} - \frac{1}{2gH}\right]^2 + \left[\frac{Nk}{g\,\hat{\omega}}\right]^2} \quad \text{(A15)}$$

Acknowledgements. The work of M. Ern was supported by the European Commission (European Union's 6th framework program) within the EC Integrated Project SCOUT-O3 (505390-GOCE-CT-2004). The work of H.-K. Cho was supported by the Korea Science and Engineering Foundation (KOSEF) through the National Research Lab. Program funded by the Ministry of Science and Technology (M10500000114-06J0000-11410). We thank the whole SABER team, in particular M. G. Mlynczak, J. M. Russell III, and L. L. Gordley for providing the excellent data set of SABER temperatures. Thanks also go to the European Centre for Medium-Range Weather Forecasts (ECMWF) for providing the global ECMWF analyses used. Helpful comments by two anonymous reviewers are acknowledged.

Edited by: P. Haynes

References

Achatz, U.: Gravity-wave breaking: Linear and primary nonlinear dynamics, Adv. Space Res., 40, 719–733, 2007.

Alexander, M. J. and Dunkerton T. J.: A spectral parameterization of mean-flow forcing due to breaking gravity waves, J. Atmos. Sci., 56, 4167–4182, 1999.

Alexander, S. P., Tsuda, T., Kawatani, Y., and Takahashi, M.: Global distribution of atmospheric waves in the equatorial upper troposphere and lower stratosphere: COSMIC observations of wave mean flow interactions, J. Geophys. Res., 113, D24115, doi:10.1029/2008JD010039, 2008.

Arkin, P. A. and Ardanuy, P. E.: Estimating climatic-scale precipitation from space: A review, J. Climate, 2, 1229–1238, 1989.

Baldwin, M. P., Gray, L. J., Dunkerton, T. J., Hamilton, K., Haynes, P. H., Randel, W. J., Holton, J. R., Alexander, M. J., Hirota, I., Horinouchi, T., Jones, D. B. A., Kinnersley, J. S., Marquardt, C., Sato, K., and Takahashi, M.: The quasi-biennial oscillation, Rev. Geophys., 39, 179–229, 2001.

Bauer, P., Lopez, P., Benedetti, A., Salmond, D., and Moreau, E.: Implementation of 1D+4D-Var assimilation of precipitation-affected microwave radiances at ECMWF. I: 1D-Var, Q. J. Roy. Meteor. Soc., 132, 2277–2306, 2006a.

Bauer, P., Lopez, P., Salmond, D., Benedetti, A., Saarinen, S., and Bonazzola, M.: Implementation of 1D+4D-Var assimilation of precipitation-affected microwave radiances at ECMWF. II: 4D-Var, Q. J. Roy. Meteor. Soc., 132, 2307–2332, 2006b.

Benedetti, A., Lopez, P., Bauer, P., and Moreau, E.: Experimental use of TRMM precipitation radar observations in the 1D+4D-Var assimilation, Q. J. Roy. Meteor. Soc., 131, 2473–2495, 2005.

Bergman, J. W. and Salby, M. L.: Equatorial wave activity derived from fluctuations in observed convection, J. Atmos. Sci., 51, 3791–3806, 1994.

Campbell, L. J. and Shepherd, T. G.: Constraints on wave drag parameterization schemes for simulating the Quasi-Biennial Oscillation. Part I: Gravity wave forcing, J. Atmos. Sci., 62, 4178–4195, 2005a.

Campbell, L. J. and Shepherd, T. G.: Constraints on wave drag parameterization schemes for simulating the Quasi-Biennial Oscillation. Part II: Combined effects of gravity waves and equatorial planetary waves, J. Atmos. Sci., 62, 4178–4195, 2005b.

Cho, H.-K., Bowman, K. P., and North, G. R.: Equatorial waves including the Madden–Julian Oscillation in TRMM rainfall and OLR data, J. Climate, 17, 4387–4406, 2004.

Dunkerton, T. J.: The role of gravity waves in the quasi-biennial oscillation, J. Geophys. Res., 102, 26053–26076, 1997.

Eckermann, S. D. and Marks, C. J.: GROGRAT: A new model of the global propagation and dissipation of atmospheric gravity waves, Adv. Space Res., 20, 1253–1256, 1997.

Eguchi, N. and Shiotani, M.: Intraseasonal variations of water vapor and cirrus clouds in the tropical upper troposphere, J. Geophys. Res., 109, D12106, doi:10.1029/2003JD004314, 2004.

Ern, M., Preusse, P., Alexander, M. J., and Warner, C. D.: Absolute values of gravity wave momentum flux derived from satellite data, J. Geophys. Res., 109, D20103, doi:10.1029/2004JD004752, 2004.

Ern, M., Preusse, P., Krebsbach, M., Mlynczak, M. G., and Russell III, J. M.: Equatorial wave analysis from SABER and ECMWF temperatures, Atmos. Chem. Phys., 8, 845–869, 2008, http://www.atmos-chem-phys.net/8/845/2008/.

Ern, M., Lehmann, C., Kaufmann, M., and Riese, M.: Spectral wave analysis at the mesopause from SCIAMACHY airglow data compared to SABER temperature spectra, Ann. Geophys., 27, 407–416, 2009, http://www.ann-geophys.net/27/407/2009/.

Ern, M. and Preusse, P.: Wave fluxes of equatorial Kelvin waves and QBO zonal wind forcing derived from SABER and ECMWF temperature space-time spectra, Atmos. Chem. Phys., 9, 3957–3986, 2009, http://www.atmos-chem-phys.net/9/3957/2009/.

Fritts, D. C. and Rastogi, P. K.: Convective and dynamical instabilities due to gravity wave motions in the lower and middle atmosphere: Theory and observations, Radio Sci., 20, 1247–1277, 1985.

Fritts, D. C. and Alexander, M. J.: Gravity wave dynamics and effects in the middle atmosphere, Rev. Geophys., 41(1), 1003, doi:10.1029/2001RG000106, 2003.

Fujiwara, M., Kita, K., and Ogawa, T.: Stratosphere-troposphere exchange of ozone associated with the equatorial Kelvin wave as observed with ozonesondes and rawinsondes, J. Geophys. Res., 103(D15), 19 173–19 182, 1998.

Fujiwara, M. and Takahashi, M.: Role of the equatorial Kelvin wave in stratosphere-troposphere exchange in a general circulation model, J. Geophys. Res., 106(D19), 22763–22780, 2001.

Fujiwara, M., Hasebe, F., Shiotani, M., Nishi, N., Vömel, H., and Oltmans, S. J.: Water vapor control at the tropopause by equatorial Kelvin waves observed over the Galápagos, Geophys. Res. Lett., 28, 3143–3146, 2001.

Garcia, R. R. and Salby, M. L.: Transient response to localized episodic heating in the tropics. Part II: Far-field behavior, J. Atmos. Sci., 44, 499–530, 1987.

Garcia, R. R., Lieberman, R., Russell III, J. M., and Mlynczak, M. G.: Large-scale waves in the mesosphere and lower thermosphere observed by SABER, J. Atmos. Sci., 62, 4384–4399, 2005.

Giorgetta, M. A., Manzini, E., Roeckner, E., Esch, M., and Bengtsson, L.: Climatology and forcing of the quasi-biennial oscillation in the MAECHAM5 model, J. Climate, 19, 3863–3881, 2006.

Hatsushika, H. and Yamazaki, K.: Stratospheric drain over Indonesia and dehydration within the tropical tropopause layer diagnosed by air parcel trajectories, J. Geophys. Res., 108, 4610, doi:10.1029/2002JD002986, 2003.

Hendon, H. H. and Woodberry, K.: The diurnal cycle of tropical convection, J. Geophys. Res., 98, 16 623–16 637, 1993.

Hines, C. O.: Generation of turbulence by atmospheric gravity waves, J. Atmos. Sci., 45, 1269–1278, 1988.

Hines, C. O.: Doppler-spread parameterization of gravity-wave momentum deposition in the middle atmosphere. Part 1: Basic formulation, J. Atmos. Sol.-Terr. Phy., 54, 371–386, 1997.

Hitchman, M. H. and Leovy, C. B.: Estimation of the Kelvin wave contribution to the semiannual oscillation, J. Atmos. Sci., 45, 1462–1475, 1988.

Holton, J. R. and Lindzen, R. S.: An updated theory for the quasi-biennial cycle of the tropical stratosphere, J. Atmos. Sci., 29, 1076–1080, 1972.

Horinouchi, T., Pawson, S., Shibata, K., Langematz, U., Manzini, E., Giorgetta, M. A., Sassi, F., Wilson, R. J., Hamilton, K., de Grandpre, J., and Scaife, A. A.: Tropical cumulus convection and upward-propagating waves in middle-atmospheric GCMs, J.

Atmos. Sci., 60, 2765–2782, 2003.
Imamura, T.: Meridional propagation of planetary-scale waves in vertical shear: Implication for the Venus atmosphere, J. Atmos. Sci., 63, 1623–1636, 2006.
Immler, F., Krüger, K., Fujiwara, M., Verver, G., Rex, M., and Schrems, O.: Correlation between equatorial Kelvin waves and the occurrence of extremely thin ice clouds at the tropical tropopause, Atmos. Chem. Phys., 8, 4019–4026, 2008, http://www.atmos-chem-phys.net/8/4019/2008/.
Jensen, E. and Pfister, L.: Transport and freeze-drying in the tropical tropopause layer, J. Geophys. Res., 109, D02207, doi:10.1029/2003JD004022, 2004.
Kawatani, Y., Takahashi, M., Sato, K., Alexander, S. P., and Tsuda, T.: Global distribution of atmospheric waves in the equatorial upper troposphere and lower stratosphere: AGCM simulation of sources and propagation, J. Geophys. Res., 114, D01102, doi:10.1029/2008JD010374, 2009.
Kiladis, G. N., Wheeler, M. C., Haertel, P. T., Straub, K. H., and Roundy, P. E.: Convectively coupled equatorial waves, Rev. Geophys., 47, RG2003, doi:10.1029/2008RG000266, 2009.
Kubar, T. L. and Hartmann, D. L.: Vertical structure of tropical oceanic convective clouds and its relation to precipitation, Geophys. Res. Lett., 35, L03804, doi:10.1029/2007GL032811, 2008.
Li, J., Wolf, W. W., Menzel, W. P., Zhang, W., Huang, H.-L., and Achtor, T. H.: Global soundings of the atmosphere from ATOVS measurements: The algorithm and validation, J. Appl. Meteorol., 39, 1248–1268, 2000.
Lindzen, R. S. and Holton, J. R.: A theory of the quasi-biennial oscillation, J. Atmos. Sci., 25, 1095–1107, 1968.
Lindzen, R. S.: The interaction of waves and convection in the tropics, J. Atmos. Sci., 60, 3009–3020, 2003.
Lopez, P.: Cloud precipitation parameterizations in modeling and variational data assimilation: A review: J. Atmos. Sci., 64, 3766–3784, 2007.
Marks, C. J. and Eckermann, S. D.: A three-dimensional nonhydrostatic ray-tracing model for gravity waves: Formulation and preliminary results for the middle atmosphere, J. Atmos. Sci., 52, 1959–1984, 1995.
Matsuno, T.: Quasi-geostrophic motions in the equatorial area, J. Meteorol. Soc. Jpn., 44, 25–43, 1966.
Mayr, H. G., Mengel, J. G., Wolff, C. L., Huang, F. T., and Porter, H. S.: The QBO as potential amplifier and conduit to lower altitudes of solar cycle influence, Ann. Geophys., 25, 1071–1092, 2007, http://www.ann-geophys.net/25/1071/2007/.
Mlynczak, M. G.: Energetics of the mesosphere and lower thermosphere and the SABER instrument, Adv. Space Res., 44, 1177–1183, 1997.
Pires, P., Redelsperger, J.-L., and Lafore, J.-P.: Equatorial atmospheric waves and their association to convection, Mon. Weather Rev., 125, 1167–1184, 1997.
Randel, W. J. and Wu, F.: Kelvin wave variability near the equatorial tropopause observed in GPS radio occultation measurements, J. Geophys. Res., 110, D03102, doi:10.1029/2004JD005006, 2005.
Ricciardulli, L. and Garcia, R. R.: The excitation of equatorial waves by deep convection in the NCAR Community Climate Model (CCM3), J. Atmos. Sci., 57, 3461–3487, 2000.
Russell III, J. M., Mlynczak, M. G., Gordley, L. L., Tansock, J., and Esplin, R.: An overview of the SABER experiment and preliminary calibration results, Proceedings of SPIE, 3756, 277–288, 1999.
Salby, M. L. and Garcia, R. R.: Transient response to localized episodic heating in the tropics, Part I: Excitation and short-time near-field behavior, J. Atmos. Sci., 44, 458–498, 1987.
Semeniuk, K. and Shepherd, T. G.: Mechanisms for tropical upwelling in the stratosphere, J. Atmos. Sci., 58, 3097–3115, 2001.
Shuckburgh, E., Norton, W., Iwi, A., and Haynes, P.: Influence of the quasi-biennial oscillation on isentropic transport and mixing in the tropics and subtropics, J. Geophys. Res., 106(D13), 14327–14337, 2001.
Spang, R., Hoffmann, L., Kullmann, A., Olschewski, F., Preusse, P., Knieling, P., Schroeder, S., Stroh, F., Weigel, K., and Riese, M.: High resolution limb observations of clouds by the CRISTA-NF experiment during the SCOUT-O3 tropical aircraft campaign, Adv. Space Res., 42, 1765–1775, doi:10.1016/j.asr.2007.09.036, 2008.
Stephens, G. L. and Kummerow, C. D.: The remote sensing of clouds and precipitation from space: A review, J. Atmos. Sci., 64, 3742–3765, 2007.
Straub, K. H. and Kiladis, G. N.: The observed structure of convectively coupled Kelvin waves: Comparison with simple models of coupled wave instability, J. Atmos. Sci., 60, 1655–1668, 2003.
Suzuki, J. and Shiotani, M.: Space-time variability of equatorial Kelvin waves and intraseasonal oscillations around the tropical tropopause, J. Geophys. Res., 113, D16110, doi:10.1029/2007JD009456, 2008.
Tindall, J. C., Thuburn, J., and Highwood, E. J.: Equatorial waves in the lower stratosphere. I: A novel detection method, Q. J. Roy. Meteor. Soc., 132, 177–194, 2006a.
Tindall, J. C., Thuburn, J., and Highwood, E. J.: Equatorial waves in the lower stratosphere. II: Annual and interannual variability, Q. J. Roy. Meteor. Soc., 132, 195–212, 2006b.
Wallace, M. W. and Kousky, V. E.: Observational evidence of Kelvin waves in the tropical stratosphere, J. Atmos. Sci., 25, 900–907, 1968.
Warner, C. D. and McIntyre, M. E.: An ultrasimple spectral parameterization for nonorographic gravity waves, J. Atmos. Sci., 58, 1837–1857, 2001.
Wheeler, M. and Kiladis, G. N.: Convectively coupled equatorial waves: Analysis of clouds and temperature in the wavenumber-frequency domain, J. Atmos. Sci., 56, 374–399, 1999.
Wu, Z., Sarachik, E. S., and Battisti, D. S.: Vertical structure of convective heating and the three-dimensional structure of the forced circulation on an equatorial beta plane, J. Atmos. Sci., 57, 2169–2187, 2000.
Yee, J. H., Talaat, E. R., Christensen, A. B., Killeen, T. L., Russell, J. M., and Woods, T. N.: TIMED instruments, J. Hopkins APL Tech. D., 24, 156–164, 2003.
Zhou, X. and Holton, J. R.: Intraseasonal variations of tropical cold-point tropopause temperatures, J. Climate, 15, 1460–1473, 2002.
Zhu, X.: Radiative damping revisited: Parameterization of damping rate in the middle atmosphere, J. Atmos. Sci., 50, 3008–3021, 1993.